2D Porous Polymers with sp2-Carbon Connections and Sole sp2-Carbon Skeletons

Jialing Kang, Senhe Huang, Kaiyue Jiang, Chenbao Lu, Zhenying Chen, Jinhui Zhu, Chongqing Yang, Artur Ciesielski, Feng Qiu, Xiaodong Zhuang

Two-Dimensional Porous Polymers with sp^2-Carbon Connections and Sole sp^2-Carbon Skeletons

Jialing Kang, Senhe Huang, Kaiyue Jiang, Chenbao Lu, Zhenying Chen, Jinhui Zhu, Chongqing Yang, Artur Ciesielski, Feng Qiu,* and Xiaodong Zhuang**

J. Kang, S. Huang, K. Jiang, C. Lu, Z. Chen, Dr. J. Zhu, Dr. C. Yang, Prof. X. Zhuang
The Meso-Entropy Matter Lab, School of Chemistry and Chemical Engineering, Shanghai Jiao Tong University, 800 Dongchuan Road, Shanghai 200240, China
E-mail: zhuang@sjtu.edu.cn, chongqing@sjtu.edu.cn
J. Kang, Prof. F. Qiu
School of Chemical and Environmental Engineering, Shanghai Institute of Technology, 100 Haiquan Road, Shanghai 201418, China
E-mail: fengqiu@sit.edu.cn
Z. Chen
College of Chemistry and Molecular Engineering, Zhengzhou University. 100 Science Avenue, Zhengzhou 450001, Henan, China.
Prof. X. Zhuang
Jiangsu Key Laboratory of Environmentally Friendly Polymeric Materials, School of Materials Science and Engineering, Changzhou University, Changzhou 213164, China. E-mail: zhuang@cczu.edu.cn
Dr. A. Ciesielski
University of Strasbourg, CNRS, ISIS UMR 7006, 8 allée Gaspard Monge, F-67000 Strasbourg, France.
Prof. A. Ciesielski
Centre for Advanced Technologies, Adam Mickiewicz University, Uniwersytetu Poznańskiego 10, 61614 Poznań, Poland

Keywords: two-dimensional, sp^2-hybridized carbon, linkage, porous polymer, polymerization

Abstract: Two-dimensional (2D) porous polymers with a planar architecture and high specific surface area have significant applications potential, such as for photocatalysis, electrochemical catalysis, gas storage and separation, and sensing. Such 2D porous polymers have generally been classified as 2D metal-organic frameworks (MOFs), 2D covalent organic frameworks (COFs), graphitic carbon nitride, graphdiyne, and sandwich-like porous polymer nanosheets. Among these, 2D porous polymers with sp^2-hybridized carbon (C_{sp^2}) bonding are an emerging field of interest. Compared with 2D porous polymers linked by B-O, C=N, or C≡C bonds, C_{sp^2}-linked 2D porous polymers exhibit extended electron delocalization resulting in unique optical/electrical properties, as well as high chemical/photostability and tunable electrochemical performance. Furthermore, such 2D porous polymers are one of the best precursors for the fabrication of 2D porous carbon materials and carbon skeletons with

atomically dispersed transition-metal active sites. In this review, the rational synthetic approaches for 2D porous polymers with C_{sp^2} bonding are summarized. Finally, their current practical photoelectric applications, including for gas separation, luminescent sensing and imaging, electrodes for batteries and supercapacitors, and photocatalysis are discussed.

1. Introduction

Materials with intrinsic porous structures (i.e., microporosity (<2 nm), mesoporosity (2–50 nm), and macroporosity (>50 nm)) have been developed for a wide range of applications, including molecular separation, gas storage, and catalysis.[1-4] Compared with inorganic porous materials (e.g., zeolites), porous polymers have gained considerable attention over the last decade because of their rich porosity, skeletons composed of light elements, tunable chemical composition, diverse functionality, processability, and well-developed synthetic methods.[5-9] On the basis of their bonding and building blocks, porous polymers have been classified into covalent organic frameworks (COFs),[10-16] metal-organic frameworks (MOFs),[17-24] covalent triazine frameworks,[25-34] porous organic polymers (POPs),[35-43] hypercrosslinked polymers,[44-53] conjugated microporous polymers (CMPs),[54-73] porous aromatic frameworks (PAFs),[74-88] polymers of intrinsic microporosity (PIMs),[89-98] supramolecular organic frameworks (SOFs),[99-102] and hydrogen-bonded organic frameworks (HOFs).[103-108] These diverse classifications overlap to some extent. Currently, research has focused on the construction of porous polymers with controlled porous frameworks and multifunctionality using new polymerization strategies. However, these porous polymers generally exhibit fair-to-poor processability as they typically precipitate directly from the organic solvent during the polymerization process, resulting in uncontrolled morphologies because of the rigid building blocks that comprise the polymeric framework. Hence, the rational design and controlled preparation of polymers with microscopic porous structures and macroscopic morphologies is of significant interest.

Porous polymers with a zero-dimensional (0D) morphology can easily be fabricated via the thermodynamic equilibrium approach to realize a low surface tension. Sparked by the discovery of graphene, porous polymers with one-dimensional (1D) and two-dimensional (2D) morphologies have gained increasing attention.[109-112] Two-dimensional porous polymers (2DPPs) have a planar architecture along with numerous attributes, including optical anisotropy, high conductivity, reversible redox properties, and a high specific surface area. This makes them promising materials for application as films for gas separation, membranes for fuel cells, thin-film electrodes for batteries and supercapacitors, and solar cells.[112-120] The preparation of single-layer 2D nanomaterials with atomic thickness on a large scale is difficult and the field of 2DPPs is broadly composed of: (1) single-layer frameworks with atomic thickness;[121,122] (2) layered structures;[123-125] (3) free-standing nanosheets;[115,126-128] and (4) sandwich-like structures with asymmetric and symmetric surfaces,[129-133] etc. With the help of efficient synthetic protocols, many 2DPPs have been well documented to date.

Currently, these 2DPPs not only have planar morphologies but also have tuneable hierarchical porous architectures. [134,135] Various functional building blocks can be efficiently incorporated into the 2DPPs framework through facile polymerization methods. Moreover, single/few-layered 2D polymers can also be obtained from layered 2DPPs via high energy shearing, e.g., ultrasonication assisted exfoliation[136,137] or ball-milling[138]. However, most reported 2DPPs have been typically based on C-N/C=N,[139-141] and B-O,[142] which have low π-delocalization that restricts their optical/electric properties and energy-related applications. In this regard, the construction of novel 2DPPs with high conductivity, low bandgaps, and exciton transport are highly desirable.

The sp^2-hybridized carbon (C_{sp^2}) bond has one valence electron on each carbon center that resides in a p_z orbital, which is orthogonal to the other three sigma bonds. Thus, C_{sp^2}-bond-based materials with continuous delocalized orbitals exhibit high electron mobility after doping with an oxidant. This has allowed for the construction of many conjugated polymers, including

polyacetylene, polythiophene, poly(*p*-phenylene vinylene), and polyfluorene. Compared with inorganic materials and small-molecule organic materials, these conjugated polymers have numerous advantages, including low weight, affordability, and flexibility. For high-performance optoelectronic applications, p- to n-type semiconductor charge transfer could be controlled in conjugated polymers via the incorporation of electron-withdrawing heteroatom moieties into the conjugated polymer framework. In addition, the conjugated polymer structure can be tuned from 0D dendritic/hyperbranched polymeric structures to 1D linear polymeric structures; however, it is difficult to realize simultaneous two-dimensional growth during polymerization to obtain the 2D layered morphologies. This can be attributed to the free rotation of chemical bonds in the building blocks and poorly reversible C_{sp^2}–C_{sp^2} coupling reactions with rapid kinetics during polymerization. Therefore, to the best of our knowledge, there are few reports on C_{sp^2} bond-based 2DPPs.

Since the first C_{sp^2}-linked 2DPP was reported in 2007[241], a large number of amorphous C_{sp^2}-linked 2DPPs have been realized via confined interfacial or solid polymerizations. Subsequently, several classical methods, including the Ullmann reaction, the Suzuki–Miyaura reaction, the Yamamoto coupling reactions, the Gilch coupling reaction, the Mizoroki–Heck reaction, and photoinduced polymerization have also been successfully used to prepare 2DPPs with C_{sp^2}–C_{sp^2} linkages. Importantly, new reactions, including oxidative polymerization reactions, sulfur-replacing reactions, dehydrogenative coupling reactions, and cyclotrimerization reactions have also been reported for the fabrication of C_{sp^2}–C_{sp^2} bond-based 2DPPs. Furthermore, inspired by the formation of the dynamic covalent bond in COFs, crystalline C_{sp^2}-linked 2DPPs have been reported via the Knoevenagel condensation and Aldol condensation reactions with reversible C_{sp^2}–C_{sp^2} linkages. While there are numerous reports on remarkable 2DPPs (e.g., graphdiyne and 2D COFs), a systematic review of the synthesis and applications of C_{sp^2}-linked 2DPPs has not yet been published. In this review article, synthetic methodologies for C_{sp^2}-linked 2DPPs have been highlighted, and they can be divided into three

sections: the solution polymerization, solid-state polymerization, and surface polymerization approaches. In each section, several polymerization methods, chemical structures, porosities, and applications of corresponding C_{sp^2}-linked 2DPPs are discussed. As shown in **Figure 1**, the milestone for different C_{sp^2}- C_{sp^2} linked 2DPPs based on different reactions are introduced. In this review, we will introduce the history of the 2DPPs based on C_{sp^2}- C_{sp^2} linkages, including a few non-2D cases for better overview of this field. In the final section, summaries of the work done on C_{sp^2}-linked 2DPPs and the challenges that need to be addressed in future work are discussed.

2. Liquid-phase polymerization approach

C_{sp^2}-linked 2DPPs are a series of quasi-two-dimensional planar porous polymers composed of covalently C_{sp^2}-linked repetitive monomers that form single layers or stacks of several layers in the perpendicular direction. Currently, the traditional carbon-carbon reactions, including the Gilch reaction, the Mizoroki–Heck coupling reaction, the Suzuki–Miyaura cross-coupling reaction, the Yamamoto coupling reaction, the Knoevenagel condensation reaction, the Aldol condensation reaction, oxidative polymerization, and the S-replacing reaction have been demonstrated as convenient approaches to realize C_{sp^2}-linked 2DPPs. While most C_{sp^2}-linked porous polymers show irregular or spherical morphologies, some notable reports on C_{sp^2}-linked 2DPPs have been published demonstrating their potential photoelectric and energy applications.

2.1. Gilch reaction

The Gilch reaction was first reported by Gilch et al.[143] in 1966 and subsequently developed by Rehahn et al.[144] It was one of the most widely used methods to realize high-molecular-weight poly(*p*-phenylenevinylenes) (PPV) (**Scheme 1A**). Because of the readily available monomers, mild reaction conditions, and facile film preparation, many PPVs have been synthesized for organic light-emitting diodes (OLEDs).[145,146]

Inspired by the facile synthesis of PPVs, Cooper et al. synthesized a mesoporous PPV network with a high surface area via the Gilch coupling polymerization of the monomer 1,2,4,5-tetrakis(bromomethyl)benzene (TBMB) in 2008 (**Figure 2**).[147] The structure of the mesoporous PPV (Figure 2a) was well characterized using solid-state NMR spectroscopy (Figure 2b). The N_2 adsorption/desorption isotherms (Figure 2c) of the mesoporous PPV collected at 77.3 K exhibited a type IV isotherm, according to the IUPAC classification. The significant H2 hysteresis loop in the desorption branch indicated a predominantly mesoporous structure. The BET surface area reached up to 761 $m^2 g^{-1}$, and the total pore volume quantified at a relative pressure of 0.99 amounted to 0.63 $cm^3 g^{-1}$. The mesoporous PPV exhibited satisfactory performance for hydrogen storage applications; however, the low synthesis yield and solubility of the bromomethyl monomers limits the preparation and application of C_{sp^2}-linked CMPs using the Gilch coupling reaction.

2.2. Mizoroki–Heck coupling reaction

In the early 1970s, Mizoroki and Heck first reported the carbon–carbon coupling reaction between aryl halides or vinyl halides and activated alkenes in the presence of a base (**Scheme 1B**) using zerovalent palladium complexes with labile tertiary phosphanes as catalysts.[148-150] Subsequently, effective and convenient methods for preparing various olefin compounds were reported using palladium complexes with high oxidation stability as catalysts via the Heck coupling reaction.[151,152] To date, the Heck coupling reaction is the most powerful method to couple aromatic halides with alkenes and the reaction conditions allow for a broader range of donors and acceptors to construct various olefin-substituted conjugated small molecules and polymers.

An important building block for the construction of various luminescent olefin-containing conjugated polymers via the Heck coupling polymerization is 1,3,5-tri(4-ethenylphenyl) benzene (TEPB). Sun et al. reported a series of luminescent microporous organic polymers

(LMOPs) by Heck polymerization of TEPB and different aromatic halides (**Figure 3**a).[153] The structure of LMOPs were well characterized by ^{1}H-^{13}C CP/MAS NMR spectroscopy. As shown in Figure **3**b, signals of phenyl and bis-substituted vinyl carbon atoms in the range of 127-141 ppm were observed in all the LMOPs, while the terminal vinyl of TEPB at ca. 114 ppm was strongly suppressed after polymerization. This indicated the successful preparation of CMP via Heck coupling polymerization. Moreover, high degrees of polymerization were achieved for all the LMOPs, as determined by the strong carbon signals from triphenylamine or tetraphenylmethane. As the solid state luminescent spectra of TEPB and LMOPs (Figure 3c), the monomer TEPB, LMOP-1, LMOP-2 and LMOP-3 show bright blue emission at 450 nm, wide emission band centred at 475 nm, green luminescence at 515 nm, red-shift emission at 458 nm compared to the emission of LMOP-3a, respectively. The luminescence of TEPB and LMOPs can be effectively quenched by picric acid, which indicates that they can be used as sensitive sensors for explosion detection. Subsequently, a one-pot preparation of LMOPs has been reported in which the Suzuki–Heck reaction with trihalide or tetrahalide-aromatic derivatives have been employed in the preparation of vinyl-substituted building blocks.[154] All of LMOPs had large specific surface areas, a narrow pore size distribution, and strong and tunable luminescence, which could be applied as fluorescent sensors for explosives detection. However, the scanning electron microscopy (SEM) images indicate that these LMOPs exhibited irregular spherical morphologies with sizes of several micrometers because of the twisted conformation of the monomers.

Zhu et al. reported a type of C_{sp^2}-linked porous aromatic framework synthesized via the Heck reaction of *p*-divinylbenzene with 1,3,5-tris(4-bromophenyl)benzene (Figure 3d).[155] The pore structure and surface area of the molecularly imprinted PAFs (MIPAFs) were adjusted by varying the content of ion-imprinted complex (Figure 3e). The BET surface area of the PAF reached up to 524 m^2 g^{-1}. The SEM images and high-resolution transmission electron microscopy (HRTEM) images demonstrated that such PAF exhibited sub-micrometre cubic

particles and had an amorphous structure which was consistent with the powder X-ray diffraction (PXRD) results. Furthermore, MIPAFs could also be constructed by incorporation of an ion-imprinted complex in the PAF architecture via the same Heck coupling polymerization. Among them, the MIPAF-11c obtained by introducing 30% ion-imprinted complex in the PAF system has good selectivity for UO_2^{2+} (Figure 3f). All in all, these MIPAFs demonstrated efficient uranium extraction with high selectivity from simulated seawater.

2.3. Suzuki–Miyaura cross-coupling reaction

The Suzuki–Miyaura reaction was first reported by Suzuki, Miyaura, and Yamada in 1979. It is a typical C-C cross-coupling reaction between aryl, alkenyl boronic acid, a boronic ester and organic halides, such as chlorine, bromine, iodoarene or olefin that is catalyzed by a zerovalent palladium complex and a suitable base (**Scheme 1C**).[156] Furthermore, potassium trifluoroborates and organoboranes have been used as reactants in place of boronic acids or boronate esters in new Suzuki–Miyaura reactions.[157] The reaction mechanism and the scope of synthetic applications were reviewed by Suzuki and Miyaura in 1995.[158]

Because of its broad functional group tolerance, mild synthetic conditions, and moderate yield, the Suzuki–Miyaura reaction has been widely used for the construction of C_{sp^2}-linked conjugated polymers. In 2008, Weber et al. firstly reported a series of poly(p-phenylene)-based CMPs synthesized by Suzuki coupling polymerization of 2,2',7,7'-tetrabromo-9,9'-spirobifluorene with various aryl-diboronic acid catalyzed by palladium acetate and triphenylphosphine as the base. This CMP exhibited a stable interpenetrating network (IPN) without phase separation, which enabled a high electroluminescence efficiency.[159] On the basis of this unique architecture, various building blocks have been incorporated for the synthesis of poly(phenylene)-based CMPs with a rigid microporous structure and high photoluminescence or two-photon fluorescence in the solid-state.[160,161] For example, a polyphenylene-based CMP (PP-CMP, **Figure 4**a-1) was synthesized whose structure was

verified by the solid-state ^{1}H-^{13}C CP/MAS NMR spectrum (Figure 4a-2) , and showed two broad peaks at 140.2 and 129.0 ppm assignable to substituted and unsubstituted phenyl carbons, respectively.[162] Besides, the energy-transfer process was also studied through transient fluorescence spectra (Figure 4a-3), indicating the time scale required for the energy transfer was on the nanosecond scale. These results showed that the energy transfer process was controlled by rapid exciton diffusion and can be used as an antenna for a light-harvesting system. In addition, the synthesized analogous CMPs showed promising applications as sensors,[163] for selective gas absorption,[164] and for organic pollutant recovery.[165] However, using the traditional Suzuki protocol, these C_{sp^2}-linked CMPs were often amorphous with a 0D morphology.

Jiang et al. reported a CMP (FeP-CMP) with a metalloporphyrin unit as the key building block synthesized via traditional Suzuki polymerization. It was composed of small 2D plate-shaped monoliths of ~100-300 nm in size.[166] For FeP-CMP (Figure 4b-1), the rigid and planar metalloporphyrin unit had a strong contribution to the realization of the 2D morphology. The PXRD results further confirmed the amorphous character of FeP-CMP. The solid-state ^{1}H-^{13}C CP/MS NMR spectrum of FeP-CMP only gave a weak and broad peak due to the high-spin paramagnetic effect. On the other hand, the free-base porphyrin CMP displayed two broad twin peaks at 127.7, 140.7 ppm and 119.3, 155.7 ppm, corresponding to the phenylene linkages and the porphyrin macrocycles, respectively (Figure 4b-2). Because of the presence of C_{sp^2}-linked iron (III) porphyrin in the skeleton, FeP-CMP was developed as a heterogeneous catalyst for efficient conversion of sulfide to sulfoxide with activated oxygen at ambient temperature and pressure (Figure 4b-3). Recently, Zhao's group proposed the use of 1,1,2,2-tetraphenylethylene (TPE) as a rigid and planar building block to construct layered porous frameworks.[167] After Suzuki cross-coupling of 1,2-diphenyl-1,2-bis(4-(4,4,5,5-tetramethyl-1,3,2-dioxaborolan-2-yl)phenyl)ethane and hexakis(4-bromophenyl) benzene that was catalyzed by tetrakis(triphenylphosphine)palladium(0), the obtained bulk C_{sp^2}-linked porous polymer (NUS-

25) powder exhibited a layered structure.[168] Ultrathin 2D NUS-25 nanosheets with a high aspect ratio were easily obtained via ultrasonic exfoliation of the bulk powder in acetonitrile Importantly, the presence of two free peripheral phenyl rings in TPE could effectively prevent re-stacking of layered NUS-25 structure. The average thickness of the NUS-25 nanosheets was ~3.0 nm, while the lateral size ranged from 2 to 20 μm. While the NUS-25 bulk powder was amorphous, the NUS-25 nanosheets exhibited small crystalline domains as determined via HR-TEM imaging. This was attributed to the eclipsed AA stacking in the few-layered microstructures. The NUS-25 nanosheets with strong fluorescence were applied as a selective chemical sensor toward acenaphthylene in various polycyclic aromatic hydrocarbons. Three C_{sp^2}-linked organic porous nanosheets (NUS 27−29) were prepared via Suzuki coupling polymerization and ultrasonic exfoliation.[169] Because of their strong aggregation-induced emission (AIE), these nanosheets could be used as fluorescent probes for in vitro live-cell imaging after encapsulation in biocompatible ZIF-8 MOFs.

2.4. Yamamoto coupling reaction

The Yamamoto coupling reaction is a common carbon–carbon coupling reaction of aryl-halide monomers with a nickel complex as catalyst, such as bis(1,5-cyclooctadiene) nickel (0) (Ni $(COD)_2$)) (**Scheme 1D**). Yamamoto et al. first reported the preparation of poly(*p*-phenylene) via dehalogenation polycondensation with Magnesium catalyzed by a nickel complex in 1977.[170] Subsequently, they continued their work advancing the Yamamoto coupling reaction.[171-173] To date, the Yamamoto coupling reaction has been widely used for the synthesis of C_{sp^2}-linked CMP networks. Compared with other coupling reactions, this polymerization method is simple and can form high-molecular-weight polyaromatics using single halogen-functionalized monomers, rendering it a notable method for the formation of C_{sp^2}-linked polymeric networks.

The first C_{sp^2}-linked CMPs bearing spirobifluorene and benzene units synthesized via the Yamamoto coupling polymerization were reported by Thomas et al., and they exhibited high surface areas of up to 1275 m^2 g^{-1}. Moreover, the surface area, pore volume, and their fluorescence properties could be effectively adjusted via copolymerization with an additional linear linker.[174] A C_{sp^2}-linked porous aromatic skeleton of PAF-1 from polycondensation of tetrakis(4-bromophenylmethane) was reported by Zhu's and Cooper's group separately. These PAF-1s had exceptional surface areas (BET surface area: 5640 m^2 g^{-1}), excellent thermal and hydrothermal stability, high gas uptake capacity (10.7 wt% at 77 K, 48 bar for hydrogen; 1300 mg g^{-1} at 298 K, 40 bar for carbon dioxide), and satisfactory organic vapor absorption performance at RT.[74,175] Many of the C_{sp^2}-linked CMPs synthesized via the Yamamoto reaction not only had high surface areas and significant chemical and thermal stability, which were beneficial for gas storage and separation applications.[176,177] Additionally, they also had tunable photoelectric properties, including for their emission wavelengths and band gaps, that demonstrated promising potential for application in organic electronics, photocatalysis, and sensing.[178]

In contrast with relatively flexible building blocks, 2D nanostructure could be readily constructed via the Yamamoto coupling polymerization of rigid units, such as TPE and porphyrin derivatives. Jiang et al. reported the synthesis of a C_{sp^2}-linked CMP containing TPE (TPE-CMP). It had strong luminescence in both the solution and solid state. This was because of the limited rotation of the structural units in the polymeric network structure.[179] TPE-CMP was amorphous as evidenced by XRD. However, it demonstrated 2D platelet-like particles, and the size of the 2D nanostructure increased from 25 nm to 255 nm with increasing polymerization time. HR-TEM images directly revealed the homogenous microporous nature of the TPE-CMP. The TPE-CMP demonstrated had pores with average size of 0.8 nm and its BET surface area reached up to 1665 m^2 g^{-1} after reaction for 72 h. They also demonstrated that the network promoted electron conjugation and stimulated exciton migration. The same group

subsequently also reported a C_{sp^2}-linked CMP (**Figure 5**a-1) via the Yamamoto reaction using diindolocarbazole as a monomer in dehydrated DMF catalyzed by bis(1,5-cyclooctadiene)nickel(0). [180] SEM imaging (Figure 5a-2) demonstrated that TCB-CMP had a 2D flake morphology with a size between 200 to 500 nm. HR-TEM imaging revealed the porous structure of TCB-CMP; it had a homogeneous micropore distribution with a size of less than 2 nm. TCB-CMP exhibited type I sorption isotherms, and its BET surface area and pore volume were calculated to be 1280 $m^2 g^{-1}$ and 0.923 $cm^3 g^{-1}$, respectively. The UV-Vis and fluorescence spectra of the polymers are shown in Figure 5a-3. The blue-emitting TCB-CMP (the inset in Figure 5a-3) and linear polymer CB-LP displayed absorption bands at 384 nm (dotted red curve) and 363 nm (black dotted line) respectively. The emission bands were observed at 468 nm with a quantum yield of 10% (solid red curve) and 445nm with a quantum yield of 0.6% (black solid line) for TCB-CMP and CB-LP, respectively. The degree of fluorescence depolarization (*p*-value) of TCB-CMP (0.0018) was lower than *p*-value of CB-LP (0.062), which facilitated the migration of excitons over three-dimensional networks. Remarkably, TCB-CMP displayed fluorescence-on and fluorescence-off chemosensing characteristics with rapid response times and a high sensitivity upon exposure to electron-rich and electron-deficient arene vapors, respectively. This was due to the synergistic effects of the C_{sp^2}-linked conjugated network and the large surface area.

Porphyrins are another rigid building blocks used for the construction of 2D conjugated polymers. Feng et al. synthesized a cobalt porphyrin-based conjugated mesoporous polymer (CoP-CMP) framework via template-free Yamamoto polycondensation of 5,10,15,20-tetrakis(4'-bromophenyl) porphyrin-Co (II) in dry dioxane under Ni $(COD)_2$ and 2,2'-bipyridyl (Figure 5b-1).[181] The Fourier transform infrared spectroscopy (FTIR) results indicated a high degree of polymerization for CoP-CMP. While the XRD results demonstrated that CoP-CMP was amorphous, it was formed by 2D ribbon-like monoliths with a high aspect ratio. The resulting CoP-CMP had a high BET surface area of ~1158 $m^2 g^{-1}$ and mesopores with a size of

~3.87 nm. Moreover, the CoP-CMP could be used as a precursor for the fabrication of nitrogen-enriched porous carbon materials with encapsulated cobalt nanoparticles (CoP-NPC) via direct pyrolysis. After thermal treatment, the CoP-NPC retained a regular ribbon-like morphology with lengths of up to tens of micrometers, widths ranging from hundreds of nanometers to micrometers, and a highly porous interconnected framework (Figure 5b-2). The TEM images show that cobalt nanoparticles with highly crystalline structure were encapsulated within graphitic carbon materials. As an electrochemical electrode, these hybrid materials showed excellent oxygen reduction reaction (ORR) catalytic activity and high stability in an O_2-saturated aqueous solution of 0.1 M KOH and 0.5 M H_2SO_4, respectively. CoP-NPC800 exhibited a positive onset potential and a high diffusion-limiting current (4.6-4.8 mA cm^{-2}) using a commercial 20 wt% platinum-carbon (Pt/C) as the standard (LSV curves was shown in Figure 5b-3). This approach provided new ideas for nano-carbon materials for fuel cells, batteries and supercapacitors. Dai et al. prepared a covalent organic polymer (COP-P-M, M = Fe, Co, or Mn) via a nickel-catalyzed Yamamoto reaction of the 5,10,15,20-tetrakis(4'-bromobiphenyl) metal-porphyrin complex (Figure 5c-1).[182] The resultant COPs were insoluble in common solvents and were amorphous because of the free distortion of phenyl rings in their monomer. For COP-P-Fe and COP-P-Co, 2D layered graphene-like structures were observed in the SEM image (Figure 5c-2). Subsequently, the carbonization of COP-P-M was demonstrated as a facile strategy to produce metal-incorporated 2D porous carbon (C-COP-P-M, M = Fe, Co, or Mn) with a rather uniform metal/nitrogen distribution and good stability in both alkaline and acid media. From Figure 5c-3, the electrocatalytic performance of the three metal-doped C-COP-P-M (M = Fe, Co, or Mn) electrodes was significantly improved compared to the metal-free C-COP-P. These C-COP-P-M have been suggested as a class of electrocatalysts for ORR. Among them, C-COP-P-Co exhibited well-defined cathodic ORR peaks for 4e oxygen reduction in O_2-saturated 0.1M KOH with a peak potential at 0.77 V. The kinetic limiting current density of C-COP-P-Co derived from the K-L plots was 13.50 mA cm^{-}

[2] at 0.75 V, which was higher than that of commercial Pt/C. This work provided a new way for the rational design and development of new and efficient ORR electrocatalysts.

Cao and Dai found that in addition to porphyrin, tris(4-bromophenyl)amine and 2,4,6-tris-(4-bromo-phenyl)-[1,3,5] triazine could also form 2D C_{sp^2}-linked CMPs (COP-4 and COP-T) when used as the rigid building blocks. This might be caused by the weak intramolecular interaction (e.g., hydrogen bonding). The locations of the nitrogen atoms and the pore sizes could be controlled in the resulting CMPs, and they were used as a precursor for well-defined N-doped porous graphitic carbon materials obtained via post-synthesis carbonization. For ORR applications, they exhibited excellent electrocatalytic activity, high stability, and low methanol poisoning. This was an approach for the construction of N-doped carbon materials for application as promising metal-free electrodes for efficient energy conversion and storage.[183,184]

2.5. Knoevenagel condensation reaction

The Knoevenagel condensation reaction is a classic organic method employed for converting an aldehyde or ketone into a cyano-substituted and cis-configuration preferred olefin using a base as catalyst (**Scheme 1E**). The Knoevenagel condensation was first carried out in high yield with an inorganic heterogeneous catalyst, such as clay and zeolite.[185] Many catalysts have been used over the past century to perform this reaction, leading to different olefin yields. Currently, organic bases (e.g., piperidine and potassium *t*-butoxide) have been considered as efficient homogeneous catalysts for the Knoevenagel condensation reaction. Compared with the noble metal-based cross-coupling reaction, this reaction is usually sustainable and inexpensive for the synthesis of C_{sp^2}-linked conjugated polymers without residual metal contaminants, which is beneficial for a wide range of photoelectric applications, such as OLEDs, solar cells, and photocatalysts. Because of its unique porous architecture, the synthesis of C_{sp^2}-linked conjugated porous polymers has been well studied via efficient metal-free-catalyzed

Knoevenagel condensation under mild reaction conditions. Because of the reversible formation of olefin linkages in the Knoevenagel condensation, some fully sp^2-carbon COFs have been reported. In this section, the C_{sp^2}-linked conjugated porous polymers obtained via Knoevenagel polycondensation have been divided into two categories according to their crystallinity.

2.5.1 Noncrystalline olefin-linked conjugated porous polymers

The conjugated polymers with a rigid skeleton have a high tendency to aggregate in a selective solvent or the solid state, leading to energy dissipation with low-emission. Cyanostilbene is an inherent AIE chromophore, which can easily be constructed via the Knoevenagel reaction of benzaldehyde and phenylacetonitrile. Chen et al. synthesized a series of solid-state emissive C_{sp^2}-linked CMPs containing cyanostilbene (CS-CMPs) by the Knoevenagel polycondensation of aldehyde-substituted monomers with 2,2'-(1,4-phenylene)diacetonitrile (**Figure 6**a) in THF and methanol using sodium hydroxide as a catalyst.[186] As shown in Figure 6b, all the polymeric networks demonstrated highly hierarchical porous morphologies comprised of spherical particles with sizes ranging from the nanometer to micrometer scale. These CMPs were amorphous powders and had BET surface areas ranging from 330 to 866 $m^2\ g^{-1}$. Because of the presence of cyanostilbene, all the CS-CMPs showed strong luminescence and their emission color and band gaps could be efficiently adjusted via the incorporation of various aldehyde-functionalized monomers, leading to tunable conjugation properties. These porous solid-emitting materials were relevant to a wide range of applications, including organic electronics, optoelectronic, sensors, and bio-imaging. Thomas's group reported the production of C_{sp^2}-linked CMFs via the Knoevenagel polycondensation of (benzene-1,3,5-triyl) triacetonitrile as the main building block with commercial terephthalaldehyde and benzene-1,3,5-tricarbaldehyde (Figure 6c and d). [187] These conjugated porous polymers had amorphous porous structures, which exhibited high CO_2 capture (90 mg g^{-1}) and selectivity over nitrogen gas (CO_2/N_2 = 96). These CMPs showed mesoporous characteristics with moderate BET

surface areas and irregular textures. The optical properties of the CMPs could be efficiently tailored via the side-chain substituents of 1,4-phenylenediacetonitrile to form intramolecular charge transfer complexes via their donor-acceptor conjugated system, demonstrating their potential application for photocatalytic hydrogen evolution. The highest HER rates for the CMPs was for TFPT-OCH_3 (22.1 μmol h^{-1}); its performance originated from its porous structure, good dispersibility in water, having the narrowest optical band gap, and strong push–pull interactions for charge separation.

In 2017, we effectively synthesized a series of conjugated porous polymers OB-POPs with many cyano-substituted fully sp^2-carbon skeletons through the polycondensation of tricyanomesitylene with different aldehyde-substituted arenes via an organic base-catalyzed Knoevenagel reaction in high yields (> 95%) (Figure 6e).[188] In contrast with the CS-based CMPs above, the XRD spectra of the OB-POPs showed two broad peaks at 2θ = 20° and 43°, indicative of the graphitic (002) and (101) diffractions, respectively. This suggested that the OB-POPs had a 2D layered structures; however, the morphologies of the OB-POPs appeared to be related to their porous structures. OB-POP-2, OB-POP-3, and OB-POP-4 revealed an agglomeration of nanoparticles (≈50 nm) in the loose texture, while OB-POP-1 showed dense-layered blocks in the size range of 5-30 μm associated with a microporous texture; this could be attributed to the relatively rigid repeat unit of the OB-POP-1 skeleton. Because of their high BET surface areas and broad visible-light absorption, these OB-POPs exhibited photocatalytic activity for hydrogen evolution from water using triethanolamine as the sacrificial electron donor and 3 wt% Pt as a cocatalyst. Here, OB-POP-3 had the highest HER of 45.4 μmol h^{-1}, which was because it had the highest apparent quantum yield (AQY) of 2.0% at 420 nm (Figure 6f). This work provided some valuable tips for designing high-performance porous polymer-based photocatalysts.

2.5.1 2 Crystalline olefin-linked 2D COFs

Construction of crystalline 2D COFs requires the formation of dynamic covalent bonds (e.g., B-O, C-N/C=N) during the polymerization process. Because classical C_{sp^2}–C_{sp^2} connections are formed via irreversible metal-catalyzed cross-coupling reactions, C_{sp^2}-linked 2D-conjugated COFs have not been realized before 2016. Our group reported the first olefin-linked 2D-conjugated COF (2DPPV) prepared via Knoevenagel polycondensation of 1,4-phenylene diacetonitrile and 1,3,5-tris-(4-formylphenyl)benzene under the catalysis of Cs_2CO_3 in *o*-dichlorobenzene (2DPPV, **Figure 7**a-1).[189] Both FTIR and X-ray photoelectron spectroscopy (XPS) confirmed the olefin-linked conjugated structure for the as-synthesized polymer framework. The OM and SEM images demonstrated sheet-like flakes with sizes ranging from a few to a hundred microns. The thickness of 2DPPV was between 50 and 300 nm. Moreover, thin nanosheets could be obtained by exfoliation via steel ball milling. HR-TEM images of the 2DPPV clearly demonstrated the ordered structure with apparent layered textures. The average distance of each layer was 0.35 nm, corresponding with the typical 2D structural characteristics for the COFs. PXRD spectra indicated the highly periodic structure of the 2DPPV with crystalline features (Figure 7a-2). Simulated XRD was carried out to further understand the stacking of the layered structure. Here, the serrated-type stacking with an "A–B–A–B" type alternating arrangement was in line with results from the PXRD and nitrogen physisorption. 2DPPV served as the ideal carbon-rich precursor for the preparation of porous carbon materials for use as an electrode for energy storage and conversion. After pyrolysis at 800 °C under an argon atmosphere, the 2DPPV-800 exhibited a low onset potential at 0.85 V *vs*. RHE for ORR, and a specific capacitance of 334 F g^{-1} at 0.5 A g^{-1} in a supercapacitor.

Jiang et al. reported the 2nd olefin-linked 2D-conjugated COF (*sp*^{2}C-COF, Figure 7b-1) constructed by the Knoevenagel polycondensation of tetrakis(4-formylphenyl) pyrene and 1,4-phenylenediacetonitrile under the catalysis of NaOH in a mixture of mesitylene/dioxane.[190] This *sp*^{2}C-COF adopted a 2D belt-like morphology. The PXRD results revealed strong

diffraction peaks, indicating the crystalline structure of *sp²*C-COF. Both experimental and calculation results suggested *sp²*C-COF adopted stacked layers with a separation of 3.58 Å, creating ordered pyrene columnar arrays and 1D nanochannels (Figure 7b-2). This extended 2D tetragon lattice with *sp²* carbon backbones along two directions led to the formation of the overlapping layer framework. Because of its fully-conjugated backbone with favorable AA-stacking, a semiconductor *sp²*C-COF with a low band gap of 1.9 eV could be oxidized by iodine vapor to form a metallic material with a conductivity of 7.1×10^{-2} S m^{-1}. The generated free radicals were bound to pyrene, forming a paramagnetic carbon structure with a high spin density. Below 10 K, a ferromagnetic phase transition was found in *sp²*C-COF, in which the spin-spin coherence developed with unidirectionally aligned spins across the material. Additionally, a series of olefin-linked 2D-conjugated COFs has been synthesized via the Knoevenagel polycondensation of tetraphenylpyrene knots with phenyl, biphenyl and terphenyl linkers, enabling the realization of as-prepared *sp²*C-COFs with different π-conjugation lengths. All of the *sp²*C-COFs adopted the AA stacking mode, with a tetragon skeleton with interweaved *sp²* carbon-conjugated backbones and tetragonal channels with theoretical pore sizes of 1.9, 2.4, and 2.7 nm, respectively, according to analysis of the experimental and simulated results. These C_{sp^2}-linked 2D COFs exhibited high stability and strong luminescence under various conditions.[191] The band gap and emission of the resulting stable framework could be adjusted by the attached monomer. Moreover, thin bright nanosheets could be peeled off from bulk powder. Subsequently, Jiang et al. [192] functionalized *sp²*C-COF with the electron-withdrawing end group 3-ethylrhodanine (ERDN) to form a D-A π-conjugated system to realize a narrow band gap, electron transfer, and exciton splitting. The unique properties of the *sp²*C-COF_{ERDN} allow them to harvest visible light for continuous and efficient production of hydrogen from water. The highest obtained HER rate was 2,120 μmol h^{-1} g^{-1} upon irradiation at wavelengths > 420, which was superior to that of state-of-the-art nitrogen-doped *g*-C_3N_4 and CTF-1.

Li et al. reported the preparation of a C_{sp^2}-linked 2D-conjugated COF (TP-COF) based on triazine as the main building block via Knoevenagel polycondensation (Figure 7c-1).[193] The SEM image shows the layered morphology of the TP-COF with sizes in the micrometer range. The PXRD profile shows intense peaks at 2.7° and 4.7° which could be attributed to the 100 and 110 crystal planes, respectively, demonstrating the AA stacking structure of the TP-COF (Figure 7c-2). TP-COF exhibited record coenzyme regeneration efficiency for the synthesis of L-glutamate from α-ketoglutarate with a yield of 97% within 12 min.

Except for end-group functionalization, optically or electrochemically active building blocks have been incorporated into the C_{sp^2}-linked 2D-conjugated COFs. Feng et al. reported a kind of C_{sp^2}-linked 2D COF (2D CCP-HATN, Figure 7d-1) constructed via the base-catalyzed Knoevenagel polycondensation of 1,4-phenylenediacetonitrile with redox-active hexaazatrinaphthalenederivative (HATN-6CHO).[194] A 2D layered framework was obtained with AA stacking (Figure 7d-2) and a BET surface area of 317 $cm^2\ g^{-1}$. To enhance the conductivity of the porous materials, 2D CCP-HATN was grown in situ on the surface of the carbon nanotubes (CNT) to obtain 2D CCP-HATN@CNT core-shell hybrids. The well-defined channels along the stacking direction facilitated fast ion diffusion and ion intercalation with redox-active of HATN. This allowed for the use of the 2D CCP-HATN@CNT as a cathode material in lithium-ion batteries (LIBs) and it demonstrated a high capacity of 116 mA h g^{-1}, excellent cycling stability, and rate capability. Wang et al. synthesized and characterized a porphyrin-based C_{sp^2}-linked 2D-conjugated COF (Por sp^2C-COF, Figure 7e-1) via polycondensation of 5,10,15,20-tetrakis(4-benzaldehyde)porphyrin and 1,4-phenylenediacetonitrile.[195] Por-sp^2C-COF had a flake-like nanoparticle morphology with strong crystalline diffraction signals, which yielded an eclipsed AA stacking in the 2D polymeric framework (Figure 7e-2). This network demonstrated a BET surface area of 689 $m^2\ g^{-1}$ and a high selective sorption of 51 for a mixture of CO_2/N_2. Considering its narrow bandgap and the photochemically-active behavior of porphyrin, Por- sp^2C-COF was applied as a metal-

free heterogeneous photocatalyst for aerobic oxidation. Under irradiation with a white LED light for 30 min, the yield of the reaction from dibenzylamine to N-benzylidenebenzylamine reached 99%. Furthermore, it exhibited a good recycling performance and tolerated various dibenzylamine with electron-withdrawing or electron-donating substituents as reaction substrates.

Recently, Zhang et al. reported the synthesis of a series of C_{sp^2}-linked 2D-conjugated COFs (*g*-CxNy-COFs) based on 3,5-dicyano-2,4,6-trimethylpyridine (DCTMP) as the main building block (Figure 7f-h).[196] After the Knoevenagel condensation reaction with 4,4”-diformyl-*p*-terphenyl (DFPTP), 4,4’-diformyl-1,1’-biphenyl (DFBP), and 1,3,5-tris(4-formylphenyl) benzene (TFPB), respectively, three 2D conjugated COFs bearing trans-olefin linkages were obtained in high yields. Intense reflection signals at 2θ between 2.62° and 26.27° were observed in the PXRD patterns, which agreed with an AA-eclipsed layer stacking model. Although the macroscopic morphology of the *g*-CxNy-COFs was not 2D, the HR-TEM images revealed a periodic porous framework containing an ordered alignment with a high degree of crystallinity, which was consistent with the PXRD analysis. These *g*-CxNy-COFs were used as photocatalysts for hydrogen generation, with *g*-$C_{40}N_3$-COF displaying the highest HER rate of 129.8 μmol h^{-1}. They also prepared a new C_{sp^2}-linked 2D-conjugated COF (Figure 7i) with a rigid planar skeleton via the Knoevenagel reaction of DCTMP and 1,3,5-tris-(4-formyl-phenyl)triazine.[197] This 2D conjugated COF possessed extended π-electron delocalization, a high surface area, and a unique nanofibrous morphology. The freestanding thin film was readily fabricated after self-assembly with single-walled CNTs; it demonstrated excellent areal capacitances of 15.2 mF cm^{-2}, a remarkable rate capability, and outstanding energy densities in micro-supercapacitors. In the latest development, Qiu et al.[198] used 2,4,6-tris(4-formylphenyl)1,3,5-triazine (TFPT) and 2,2’,2’’-(benzene-1,3,5-triyl)triacetonitrile (BTAN) to synthsize two sp^2 carbon-conjugated COFs: TFPT-BTAN and TFPT-BTAN-AO (Figure 7j). Remarkably, TFPT-BTAN-AO with good chemical, thermal, and radiation stability shows

excellent ability to absorb UO_2^{2+}. Such method opens the way for the detection and extraction of heavy metal ion containing pollutants.

2.6. Aldol condensation reaction

In general, the strong electron-withdrawing substitution of nitriles appended by olefin linkage during the Knoevenagel condensation reaction might lead to instability of the C_{sp^2}-linked 2D-conjugated COFs. The star-shaped 2,4,6-tri((E)-styryl)-1,3,5-triazine (TST) constructed via the reversible Aldol condensation reaction of 2,4,6-trimethyl-1,3,5-triazine (TMT) and benzaldehyde (**Figure 8**a) was reported by Fang et al.[199] and Meier et al.[200] Inspired by these works, Zhou et al. synthesized a novel fluorescent triazine-based covalent organic polymer (COP-1) using TMT and phthalaldehyde as monomers. Semi-crystalline COP-1 could be used as a fluorescent sensor for HCl and NH_3 gases.[201] In 2019, Yaghi et al. reported the first unsubstituted olefin-linked 2D COF (COF-701 in Figure 8b) created by linking TMT and 4,4'-biphenyldicarbaldehyde (BPDA) via Brønsted acid-catalyzed Aldol polycondensation.[202] The wide-angle X-ray scattering (WAXS) results indicated high crystallinity COF-701, with a staggered AB stacking mode (Figure 8c). The SEM image indicated the presence of COF-701 particles. Because of the high specific surface area (1715 $m^2\ g^{-1}$) and high stability in acidic and basic conditions, COF-701 could be used to immobilize the strong Lewis acid $BF_3{\cdot}OEt_2$ in its pores and yield BF3⊂COF-701, which served as heterogeneous catalysts for the Diels−Alder reaction (Figure 8d).

Zhang et al. reported two unsubstituted olefin-linked 2D COFs (*g*-$C_{18}N_3$-COF and *g*-$C_{33}N_3$-COF) synthesized via polycondensation of TMT with DFBP and TFPB, respectively.[203] According to the experimental PXRD and simulation results, the crystalline *g*-$C_{18}N_3$-COF and *g*-$C_{33}N_3$-COF demonstrated an eclipsed AA layer stacking, surface areas of 1170 $m^2\ g^{-1}$ and 752 $m^2\ g^{-1}$, respectively, and one prominent distribution peak were observed for both *g*-$C_{18}N_3$-COF and *g*-$C_{33}N_3$-COF. Moreover, *g*-$C_{33}N_3$-COF showed photocurrents of ~45 μA cm^{-2} at 0.2

V *vs.* RHE when used as a photoelectrode, which can be used for photocatalytic hydrogen generation.

2.7. Oxidative polymerization reaction

Oxidative polymerization is an efficient method for preparing porous polymers with C_{sp^2}–C_{sp^2} connections. It involves building blocks containing thiophene, pyrrole, or aniline end-groups with strong oxidants (e.g., ammonium persulfate and $FeCl_3$) in anhydrous solvents. Oxidative reaction with $FeCl_3$ usually has a short reaction time and a high yield, allowing for polymerization with a more simple and convenient approach than others. Thomas et al. first described the synthesis of a microporous conjugated poly(2,2',7,7'-tetrathienyl-9,9'-spirobifluorene) based on thiophene linkages (**Figure 9**a).[204] These polymers could fill the pores of the conjugate network to create an IPN with a controlled structure. Because their covalent microporous organic networks had many sulfur ligands as metal-binding sites, various catalytically activity nanoparticles effectively grew on the pore walls of these polymers, and they could be applied as heterogeneous catalysts. In the same year, Yu et al. reported the oxidative polymerization of spirobifluorene with terminal thiophene groups to form a C_{sp^2}-linked CMP.[205] The hydrogen adsorption capacity of the obtained materials was proportional to the surface area. However, the sulfur atoms had no significant effect on the hydrogen adsorption. To enhance their adsorption capacity at an ambient temperature, new C_{sp^2}-linked CMPs (PTTPP) have been prepared via oxidative polymerization using thiophene-functionalized porphyrin as a monomer.[206] These CMPs showed a high specific surface area of 1522 $m^2\ g^{-1}$ and a hydrogen absorption capacity of 5.0 mass% H_2 at 77 K and 65 bar. The porphyrin core provided coordination sites for a variety of transition-metal ions. For example, P(Fe-PTTPP) revealed a slight increase in the heat of adsorption for hydrogen. Moreover, other works have also reported various C_{sp^2}-linked CMPs prepared via oxidative polymerization of

thiophene or carbazole functionalized monomers, which were applied for gas storage,[62] optoelectronic devices,[207] and explosive detection.[208]

However, most C_{sp^2}-linked CMPs constructed via oxidative polymerization do not feature controlled 2D morphology because of the flexible structure of their monomers. To overcome this issue, Liu et al. synthesized a highly conductive 2D porphyrin COF (TThPP) on the surface of copper foils using tetrakis (4-thiophenephenyl) porphyrin (TThP) as a monomer through oxidation polymerization (Figure 9b and c).[209] The TThPP film composed of flat nanosheets completely covered the surface of the copper foil (Figure 9d). The thickness of the TThPP film was ~1.2 μm. Ultrathin TThPP nanosheets with a thickness of 3.8 nm could be achieved via exfoliation of the as-prepared film, which was further confirmed by AFM imaging. The arrangement of the laminated sheets of TThPP greatly facilitated carrier transport, layered storage of lithium ions, and electrolyte transport. Figure 9e showed CVs of TThPP electrode mixed lithium-ion capacitor (LIC) at different scanning rates. The CV curve at the low scanning rate of 5 mV s^{-1} is almost rectangular, indicating the ideal capacitance behaviour. The galvanostatic charge–discharge voltage curves (Figure 9f) of LIC in the range of 1.8-3.8 V at different current densities showed the curve close to the triangle, indicating the excellent capacitive behaviour of LIC. Besides, the TThPP film exhibited a high specific capacity of 666 mA h g^{-1} at a current density of 200 mA g^{-1} as a LIB anode, and a specific capacitance of 82.79 F g^{-1} at a current density of 50 mA g^{-1} as a supercapacitor anode. These results represent the application of C_{sp^2}-linked 2D COFs as next-generation electrode materials.

The advantages of the oxidative polymerization method include a low cost, mild reaction conditions, use of a single monomer without extra substitutes, and easy scale-up. Oxidative polymerization can be easily used to prepare conjugated porous polymers with C_{sp^2}–C_{sp^2} connections but they have difficulty realizing 2D morphologies. Even when a 2D morphology was achieved, the ordering of the 2D nanosheets was unclear. Because of the uncontrollable

and fast polymerization, this was not the best approach to realize 2D porous polymers, except for 2D templates[210] or for interfacial polymerization.[211]

2.8. S-replacing reaction

Poly(isothianaphthene) (PPA-S) with C_{sp^2}–C_{sp^2} connections could be constructed efficiently using phthalic anhydride as the starting material with Lawesson's reagent (P_4S_{10}). To discover new approaches for synthesis of C_{sp^2}-linked 2D conjugated porous polymers, we developed a new type of sulfur-enriched conjugated polymer nanosheet 2DP-S (**Figure 10**a) via an S-replacing synthesis approach.[212] The as-prepared 2DP-S comprised quinoidal polythiophene and *p*-phenylenevinylene along the horizontal and vertical directions, respectively. The SEM images in Figure 10b shows many free-standing 2D sheets with sizes up to several micrometers, suggesting a high aspect ratio of up to ~400. A uniform thickness of 7.0 ± 1.0 nm indicated the formation of an ultrathin polymeric layer of 2DP-S nanosheets. However, XRD analysis of 2DP-S revealed two broad peaks at 24.5° and 43°, indicating amorphous carbon, which may be ascribed to the nonplanar structure due to hindrance by S atoms. Such C_{sp^2}-linked polymer nanosheets could be further used as carbon precursors for the direct construction of N/S co-doped porous carbon nanosheets (N/S-2DPC) with controlled N/S ratios and high specific surface areas of 1153 $m^2\ g^{-1}$ via high-temperature treatment and ammonia activation (Figure 10c). They were applied as electrochemical catalysts for ORR. Among them, N/S-2DPC-60 showed an ORR peak-potential of 0.65 and an onset-potential of 0.77 V in O_2-saturated 0.1 M KOH. By studying the relationship between the N/S ratio and the ORR performance (Figure 10d), a higher diffusion current density and a more positive initial potential can be found in N/S co-doped 2DPCs, indicating N/S-co-doped 2DPCs superior to S-doped porous carbon nanosheets. In 2DPCs, an ultralow half-wave potential (0.75 V *vs*. RHE) and the highest nitrogen content (5.39 wt%) of N/S-2DPC-60 showed that nitrogen doping has a positive effect on ORR performance. To investigate the crossover effects, the electrocatalytic selectivity of the

fuel molecule methanol to N/S-2DPC-60 and Pt/C was performed (Figure 10e). When methanol (v/v, 2%) was added, the current of N/S-2DPC-60 barely changed, while the current of Pt/C dropped sharply to negative, suggesting that N/S-2DPC-60 is better than commercial Pt/C catalysts in avoiding cross effects. Furthermore, N/S-2DPC-60 was also employed to construct a Zn–air battery with a power density of 0.69 mW cm^{-2} at a current density of 2.1 mA cm^{-2}. These results indicated that such method of preparing porous carbon nanosheets with high specific surface area and controllable N/S ratio offers new approach for high performance batteries, supercapacitors, etc.

2.9. Interfacial synthesis

The interface is a natural planar surface for the construction of 2D polymeric nanostructures, such as 2D polyimide[213] and 2D polyaniline[214]. Interfacial synthesis is a new method for synthesis of new 2D materials. At present, researchers have reported the latest research progress on the construction of nano-building materials on interface. [215,216] As shown in **Figure 11**a-1, in the presence of Pd catalyst and base, 2D COF can be prepared by interfacial method via Suzuki reaction. The reaction can be divided into two phases: the aqueous phase containing the inorganic base and the organic phase containing the catalyst (Figure 11a-2). During the reaction, the components in the organic phase meet the organic base in the aqueous phase at the interface to begin the transfer of metallization. Since the hydroxide/halogen exchange or hydroxylation of the borate ester group in this step is reversible (Figure 11a-3), the entire polymerization can be kept in equilibrium by low temperature, thus giving the product an internal order. Li et al. reported the synthesis of two C_{sp^2}-linked 2D conjugated COFs films (2DCCOF1 and 2DCCOF2) at the liquid–liquid interface via Suzuki reactions under relatively mild conditions (Figure 11b-1, c-1).[217] During the polymerization process, the reaction occurred exclusively when the metal transferred and contacted the inorganic base in the aqueous phase at the liquid–liquid interface. After slow polymerization at a low temperature (2 °C) for a month, large, stable

sheets with high fluorescence under the UV light were obtained, indicating the successful formation of a conjugated polymer system via the Suzuki reaction. Optical microscopy (OM) showed that the two films were flat thin sheet with cracks and mm-sized in the lateral direction. AFM images also demonstrated the flat nature of 2DCCOF1 and 2DCCOF2 with thickness of 18 nm and 23 nm, respectively. The films have straight edges, indicating the presence of crystalline facets. For 2DCCOF1, HR-TEM imaging demonstrated a layered structure with 2D periodicity (Figure 11b-2). The fast Fourier transformation (FFT) revealed a hexagonal pattern and the spots matched with the simulated diffraction pattern of a structure with A-B-C stacking (Figure 11b-3). Thinner 2DCCOF1 sheets could be exfoliated in N-methyl-2-pyrrolidone (NMP) via ultrasonication. In contrast, 2DCCOF2 adopted a stair-like multi-layer structure and orthogonal features at the edges, which indicated a square lattice with a d-spacing of 1.1 nm in small domains from the low-magnification TEM image (Figure 11c-2). The FFT pattern also revealed a similar square periodicity with AB aggregation in the 2DCCOF2 film (Figure 11c-3). When used as the channel material in a field-effect transistor (FET), the carrier mobility of C_{sp^2}-linked 2DCCOF1 could reach up to 3.2×10^{-3} cm^2 V^{-1} s^{-1}, which was three orders of magnitude larger than C=N linked 2D COF films. Furthermore, 2DCCOF1 also exhibited comparable electrochemical hydrogen evolution reaction (HER) activity via horizontal deposition on a copper electrode.

3. Solid-state polymerization approach

Solution polymerization methods involving various metal catalysts usually suffer from a lack of control over the degree of polymerization and limited small-scale production for the synthesis of C_{sp^2}-linked conjugated porous polymers, which limits their further industrial applications for photo/electrochemical-catalyzed energy storage and conversion. Compared with solution polymerization, solid-phase polymerization allows formation of conjugated polymers with a well-defined structure and provides multi-dimensional control over the

polymerization direction. Moreover, solid-phase polymerization process is not significantly affected by the solvent and catalyst.[218] Hence, solid-state polymerization has been demonstrated as one of the best approaches to realize C_{sp^2}-linked 2D conjugated porous polymers. The solid-state polymerization methods presented in this section have been divided into two parts that discuss thermally-initiated endogenous polymerization reactions and photoinduced polymerization reactions.

3.1. Thermally-induced endogenous polymerization reaction

Generally, the dehalogenation temperature for halogenated aromatic hydrocarbons is as high as 700 °C. Most aromatic hydrocarbons are unstable at high temperatures, however, endogenous solid-phase polymerization is hard to be carried out to realize novel structures.[218] To verify whether pre-arranged monomers can promote the conversion of crystals to polycrystals, Loh et al. prepared crystalline 2D-conjugated aromatic polymers (2D-CAP) driven by a endogenous solid-state C_{sp^2}–C_{sp^2} coupling polymerization of 2,7,13,18-tetrabromodibenzo[a,c]dibenzo[5,6:7 uinoxalineino-[2,3-i]phenazine (2-TBQP) (**Figure 12**a).[219] For this, 2-TBQP was first sublimed and recrystallized in a tube furnace to obtain 2-TBQP needle-like single crystals that were millimeters to centimeter in size. Single-crystal XRD results indicated that 2-TBQP had a packed lamellar structure with face-to-face stacking, indicating strong π–π interaction at a distance of 3.269 Å. Furthermore, the zigzag packing of each unit cell favors the debromination reaction, and thus the concomitant C_{sp^2}–C_{sp^2} coupling reaction. Because of the high thermal stability of the phenazine ring-fused compound, a gray needle-like crystalline polymer (2D-CAP) was obtained via debromination of the red single crystal (2-TBQP) at 520 °C for 6 h. As presented in the SEM image, the 2D morphology with a layered structure of 2D-CAP is similar to that of the 2-TBQP crystal. Exfoliation of nanosheets using Scotch tape revealed triangular sheets with a length of 15 microns and neat edges (Figure 12b). AFM further confirmed the sheet-like structure with neat edges and a sheet

thickness of ~1 nm, similar to single-layered graphene (Figure 12c). In the XRD pattern, the diffraction peaks at 6.2° and 26.7° were assigned to the (110) and (002) plane, respectively, which demonstrated satisfactory agreement with simulation results (Figure 12d). The experimental XRD results demonstrated the good crystalline order of layered 2D-CAP with an AA-eclipsed stacking, which agreed with the simulated results. The as-prepared 2D-CAP showed a type I isotherm, indicating significant micropores with a homogeneous diameter of 0.6 nm. The BET surface area of 2D-CAP reached 539 $m^2 g^{-1}$. On application as the anode in a sodium battery at room temperature, a stable capacity, high rate capability as well as long-term cycling stability could be obtained because of the rapid charge and discharge of sodium ions with 2D-CAP (discharge–charge profiles in Figure 12e).

Loh et al. also reported two important C_{sp^2}-linked 2D conjugated porous polymers via the thermal debromination of 2,7,11,16-tetrabromotetrabenzo[a,c,h,j]phenazine (2-TBTBP] and 3,6,14,17-tetrabromodibenzo[a,c]dibenzo[5,6:7,8]-quinoxalino-[2,3-i]phenazine (3-TBQP) at 520 °C for 3 h.[220] The polymerization yield of 2-TBTBP and 3-TBQP were ~48% and ~61%, respectively, which was near the theoretical values (51.68% and 59.95%). This suggested that the solid-state C_{sp^2}–C_{sp^2} coupling polymerization method had a high conversion of brominated monomers. In particular, CAP-2 (Figure 12f) de-brominated from 3-TBQP retained its original needle shape with lamellar features, which was similar to its precursor. Additionally, the CAP-2 could be mechanically exfoliated into few layered flakes using Scotch tape. The lateral size of the exfoliated CAP-2 sheets was ~6 μm with neat edges. The AFM height profile revealed that this sheet was ~4 nm thick and comprised of ~10 layers. As shown in Figure 12g, asymmetric supercapacitors were studied in a potential window of 0-1.6 V. Similar to the three-electrode battery, the current density increases with the increase of the scan rate. Even at high scan rates (100 mV s^{-1}), the battery showed good energy storage rate capability. The nanocrystalline 2D CAP-2 exhibited a distinct layered structure with a high regular pore size in the range of 0.7–1.0 nm and a high electrical conductivity of 6.0×10^{-5} S cm^{-1}, which facilitated

its application in supercapacitors. As the positive electrode in a three-electrode system, CAP-2 provided a specific capacitance of 233 F g^{-1} at a current density of 1.0 A g^{-1} in a 2 M KCl electrolyte (Figure 12h). CAP-2 also had excellent cycle life and capacity retention of ~80% over 10,000 cycles. These results demonstrated that thermally-induced endogenous polymerization is a simple approach to prepare C_{sp^2}-linked conjugated porous polymers with a regular pore size and a 2D planar structure under catalyst-free and solvent-free conditions. The as-prepared materials had promising performance in applications for energy storage and conversion, like batteries and supercapacitors; however, the harsh solid-state polymerization conditions limited the monomers that could be used to prepare C_{sp^2}-linked 2D conjugated porous materials.

3.2. Photoinduced polymerization reaction

Besides thermal stimulus, light irradiation is another non-contact method that can trigger chemical reactions in the solid state to form C_{sp^2}–C_{sp^2} connections (**Scheme 1F**). For instance, anthracene and its derivatives have rich photophysical and photochemical properties. They have been applied to a wide range of systems, including energy migration probes and sensors, triplet sensitizers, and photochromic substrates for 3D memory materials.[221] Importantly, the photodimerization of anthracene under UV irradiation results in a considerable change of its physical properties.[222] Hence, the photodimerization method is a facile approach for the preparation of 2D porous conjugated polymers with C_{sp^2}–C_{sp^2} connections.

Sakamoto et al. first reported the rational synthesis of ordered, free-standing monolayered 2D conjugated polymer sheets with internal periodicity composed of areal units. This was accomplished by the crystallization of a photoreactive monomer containing 1,8-diethynylanthrylene and a subsequent photo-polymerization process (**Figure 13**a and b).[223] A single crystal of monomers was composed of layers parallel to each other. Therefore, the two-dimensional organization could be well-controlled because of the low molecular motion of the

lattice; hence, lateral polymerization occurred in a predefined manner (Figure 13c and d). The crude polymeric sheets could be purified by washing with an organic solvent (e.g., TCE) to remove unreacted monomer crystals, and the obtained pure cross-linked polymeric sheets were stable even at 80 °C for 1 day. Individual monolayers could be exfoliated from the pure polymeric sheet with lateral dimensions of 1-2 μm and a uniform thickness of 2.5 nm via heating at 150 °C in NMP. Later, Sakamoto et al. reported the synthesis of a series of 2D conjugated porous polymers via [2+2] photocycloaddition.[224-229] While 2D conjugated porous polymers with C_{sp^2}–C_{sp^2} connections are easily achieved via the solid-state photoinduced polymerization approach, most of these polymers were not fully C_{sp^2}-conjugated systems because sp^3-carbon was present after cyclization between alkyne and anthracene.

4. On-surface polymerization approach

Over the past decade, on-surface synthesis has been regarded as an effective bottom-up approach to construct new conjugated molecules,[230] including 0D, 1D, and 2D materials. Well-defined graphene nanoribbons have been reported by covalently coupling small reactive precursors on lattice surfaces under ultra-high vacuum (UHV) upon thermal treatement.[231] Additionally, this method has advantages that include: (1) the formation of irreversible and stable covalent bonds endows the molecule with high thermal stability; (2) covalent assembly facilitates electronic transport, making the network suitable for numerous applications; (3) compared with reactions in solution, this is a solvent-free reaction with high level control of the molecules and substrates at the atomic level, allowing for a precise molecular structure over a large temperature range; (4) the in situ reaction products on the surface of the substrate is convenient for their practical application, mitigating the solubility issues that often accompany solution syntheses; (5) scanning probe microscopy is facile tool for characterization and manipulation of the obtained molecules and materials.[232, 233] In this section, we introduce on-surface preparation methods for 2D conjugated porous polymers with C_{sp^2}–C_{sp^2} connections and

C_{sp^2}-based skeletons, including the Ullmann coupling reaction, the cyclotrimerization reaction, the dehydrogenative coupling reaction, and the condensation reaction.

4.1. Ullmann coupling reaction

The Ullmann reaction is a kind of copper-catalyzed C_{sp^2}–C_{sp^2} dehalogenation reaction for the synthesis of symmetric biaryls first reported in 1901.[234,235] Typically, two molar equivalents of aryl halide reacted with one molar equivalent of copper at high temperatures (> 200 °C) to form one molar equivalent of diaryl molecules and copper halide (**Scheme 1G**). Currently, various aryl halides with nucleophilic substituents (e.g., phenoxides) have been used as functional reactants in copper-catalyzed Ullmann-type reactions. The mechanisms of the Ullmann coupling reaction has been reviewed in detail by Bent et al. in 1993.[236] Subsequently, Hla et al. used scanning tunneling microscope (STM) to investigate the Ullmann reaction in a UHV chamber on the Cu (111) facet in a step-by-step manner.[237] In addition, researchers found that Au (111), Ag (111), Ag (110) and highly oriented pyrolytic graphite could also be used for Ullmann reactions.[238-240]

In 2007, Grill et al. reported the synthesis of C_{sp^2}-linked 2D conjugated polymeric nanostructures via the Ullmann reaction of tetra(4-bromophenyl) porphyrin (Br_4TPP) with halides on Au (111) at a high temperature (**Figure 14**a).[241] For this, the porphyrin-based monomer was first deposited on the surface at room temperature; dissociation of the substituent Br atoms on the Br_4TPP occurred when the sample was annealed at 590 K and macromolecular nanostructures of various shapes formed on the surface via intermolecular C_{sp^2}- C_{sp^2} linkage of the monomers (Figure 14a and b). To obtain porphyrin frameworks with 2D patterns, a monomer with four possible connections was required. By changing the number and the relative position of the bromine atoms on the porphyrin-based molecule, the nano-architecture of the macromolecular structure on connection between the molecules on Au (111) could be controlled. These structures include dimers, 1D linear polyporphyrins, and 2D polyporphyrins.

The resulting C_{sp^2}-linked 2D polyporphyrin should realize fast charge transfer on the molecular building blocks. They could have potential applications as new functional materials for use in the electronic, optical or magnetic sciences. Because of the different dissociation energies of the halogen substituents, Grill et al. reported a strategy for the preparation of C_{sp^2}-linked conjugated porous polymers in a hierarchical manner.[242] The 5,15-bis(4'-bromophenyl)-10,20-bis(4'-iodophenyl)porphyrin (trans-Br_2I_2TPP) molecules proceeded through two sequential steps to form a 2D conjugated network from the 1D linear nanostructure on the Au (111) on heating at 120 °C and further heating at 250 °C. The fabrication of heterogeneous nanostructure with high selectivity was realized via the Ullmann coupling reaction of trans-Br_2I_2TPP with dibromoterfluorene. Moreover, the substrate-directed growth of C_{sp^2}-linked 2D polyporphyrin nanostructures was also achieved on the anisotropic Au (100) surface.

Halogenated metalloporphyrins are satisfactory building blocks for the preparation of expanded 2D polymer sheets with high chemical and mechanical stability, as further confirmed by Smykalla et al.[243] Unfortunately, all of aforementioned cases demonstrate a rather low degree of polymerization. Fasel et al. reported a well-ordered 2D covalent network with a fully C_{sp^2}-based skeleton from an iodinated cyclohexa-*m*-phenylene (Figure 14c).[244] This molecule represented a typical monomer for the construction of porous graphene, featuring a C_{sp^2}-linked covalent conjugated network with a low defect density. Moreover, the dehalogenation reaction of iodinated cyclohexa-*m*-phenylene via the Ullmann coupling reaction on (111) surfaces of various metals had been investigated. Figure 14d shows STM images of the C_{sp^2}-linked polyphenylene networks with different morphologies supported on Cu (111), Au (111), and Ag (111). A branched morphology with low-density clusters was found on Cu (111) (Figure 14d-1), while small 2D compact domains were observed on the Au and Ag surface (Figure 14d-2,3). A more ideal 2D polyphenylene with highly ordered networks was achieved on the silver surface after polymerization at 825 K for 5 min. DFT simulations indicated that the balance

between the diffusion and intermolecular coupling had a large influence on the morphology of 2D polyphenylene on the surfaces of these metals.

Perepichka et al. reported atomic-layer thin 2D π-conjugated porous polymers through Ullmann coupling on Ag (111) using tetrabromotetrathienoanthracene (TBTTA) as the monomer under UHV conditions (Figure 14e).[245] After annealing at 300 °C for 10 min, a porous network of P^2TTA with low-range order was observed via STM (Figure 14f). The high-resolution STM micrographs indicated the presence of two kinds of adjacent building blocks with short (1.2 ± 0.1 nm) and long (1.5 ± 0.1 nm) connections, attributed to the linkage of P^2TTA and the organometallic network by TTA–Ag–TTA bonding. The HOMO of the 2D conjugated network was shifted towards the Fermi level by 0.6 eV on polymerization, suggesting the controlled construction of C_{sp^2}-linked 2D conjugated polymers with tailored band-gaps. 1,3,5-tris(4-bromophenyl)benzene (TBPB) is another important building block for the preparation of C_{sp^2}-linked 2D conjugated polymers via the Ullmann coupling reaction. Gutzler et al. reported the reticular synthesis of 2D conjugated COFs built from TBPB on the surface of Cu (111) under UHV conditions. After annealing to 300 °C, hexagonal patterns with distances of 1.24 ± 0.06 nm were observed, indicating the transition of TBPB from a protopolymer to a C_{sp^2}-linked 2D disordered COF.[246] Beton et al. also investigated the C_{sp^2}-linked 2D conjugated polymer from TBPB via the Ullmann coupling reaction on an Au (111) substrate.[247] The TBPB could self-assemble as an ordered, close-packed array on the surface of Au, which transformed into 2D conjugated network consisting of quadrilateral to octagonal polygons. This 2D conjugated porous polymer could serve as a host to capture sublimed C60. Recently, Gutzler et al. reported the synthesis of C_{sp^2}-linked 2D conjugated COF from TBPB on the two interfaces of *h*-BN/Ni (111) and graphene/Ni (111).[248] Unfortunately, the well-defined nanostructure 2D conjugated COF with long-range order was still not observed. Lackinger et al. demonstrated that hierarchical Ullmann coupling polymerization of 1,3-bis(*p*-bromophenyl)-5-(*p*-iodophenyl)benzene was better than direct polymerization to achieve a 2D

conjugated porous polymer with a densely packed nanostructure and a uniform single pore.[249] The influence of the reaction parameters like surface temperature, and heating and deposition rates on the morphologies observed via STM were in agreement with the simulation results. The thermodynamic and kinetic mechanisms of the Ullmann reaction on gold and silver surfaces have been also been well-studied by Lackinger et al.[250]

4.2. Cyclotrimerization reaction

The transition metal-catalyzed [2+2+2] cyclotrimerization reaction is a powerful method for one-pot construction of various complex polycyclic aromatic hydrocarbons with a high yield (**Figure 15**a).[251,252] Liu et al. reported the synthesis of C_{sp^2}-linked conjugated microporous polyphenylenes with tunable pore size via the ethynyl [2+2+2] cyclotrimerization using inorganic dicobalt octacarbonyl nanoparticles as catalyst.[251] These porous polymers had BET surface areas higher than 1000 $m^2\ g^{-1}$, which could be used as functional materials for efficient hydrogen capture. However, this reaction had regioselectivity issues, leading to uncontrolled morphologies. To realize conjugated porous polymers with 2D morphologies, Lackinger et al. investigated the on-surface polymerization of 1,4-diethynylbenzene (DEB) monomers on Cu (111) via the cyclotrimerization reaction.[253] DEB showed well-ordered self-assembly on the surface of Cu (111). However, disordered 2D covalent networks with complex structures were observed after thermal activation. Thus, the exploration of C_{sp^2}-linked 2D conjugated organic nanostructures on different metal surfaces and crystallographic orientations of the monomers is highly desirable.

Fasel et al. reported a 2D polymer with a honeycomb structure via on-surface cyclotrimerization reactions of 1,3,5-tris-(4-ethynylphenyl) benzene (TEB) on Au (111) (Figure 15b).[254] Upon annealing the TEB/Au (111) sample at 433 K, STM images revealed a fully C_{sp^2}-linked interconnected porous network with a pore-to-pore distance of 1.7 ± 0.1 nm, which was consistent with the 2D polyphenylene structure (Figure 15c). On increasing the annealing

temperature to 523 K, the similar conjugated networks were unaltered. Compared with Ag (111) and Cu (111), the yield of the cyclotrimerization was high and reached up to 75% on the surface of Au (111), possibly because of the efficient formation of a metallacyclopentadiene intermediate. Gao et al. investigated the cyclotrimerization of 4,4'-diethynyl-1,1'-biphenyl (DEBP) on the Au (111) surface by combining STM measurements with DFT calculation (Figure 15d).[255] As illustrated in Figure 15e-1, the monomer of DEBP was first self-assembled into ordered structures on the atomically flat Au (111) surface. During annealing at 100 °C, triple bonds of DEBP were cyclotrimerized into one benzene ring to form the C_{sp^2}-linked 2D polymeric networks (Figure 15e-2). From Figure 15e-3 to Figure 15e-5, the coexistence of symmetric 1,3,5- and asymmetric 1,2,4-trisubstituted benzene rings was observed via cyclotrimerization of diyne monomers. Moreover, the ratio of the regioselectivity was 5.6:1, which was higher than that of solution polymerization. This indicated that the synthesis of the 1,2,4-isomeric structure was suppressed by the surface-assisted cyclotrimerization on Au (111).

Chi et al. presented a type of surface-assisted cyclotrimerization for the construction of a C_{sp^2}-linked 2D conjugated polymeric network from acetyl-substituted molecules on the surface of Ag (111) under UHV (Figure 15f).[256] After deposition of 1,3,5-tris(4-acetylphenyl)benzene (TAPB) on the metal surface, irregular conjugated porous networks with zigzag edges and similar heights of TAPB were observed (Figure 15g). The HR-STM demonstrated an extended pyramidlike structure involving ten molecules, which was realized by the dimerization coupling of adjacent acetyls and cyclotrimerization coupling of trifunctional acetyls (Figure 15h-i), which was further confirmed by the XPS spectra. The pore-to-pore distance of the nanopores was 14.9 ± 0.2 Å, in agreement with the calculated value for the 2D polyphenylene structure. This is a universal strategy for the preparation of a C_{sp^2}-linked 2D polymeric network from acetyl-substituted molecules from alternate metal substrates, including Au (111) and Cu (111).

4.3 Dehydrogenative reaction

As aforementioned, the cyclotrimerization of arylalkanes often suffers from unwanted by-products on the surfaces during the surface-assisted polymerization of C_{sp^2}-linked 2D conjugated polymeric networks. The harsh synthetic conditions of these monomers limit their applications for optical and electric devices. The metal-catalyzed aromatic C-H bond activation of aromatic molecules for the construction of conjugated polymers with C_{sp^2}–C_{sp^2} bond has attracted significant interest.[257] Recently, cross-dehydrogenative coupling reactions with various transition-metal catalysts exhibited both regio- and enantio-selectivity.[258] Thus, the direct C-H activation of aromatic groups with multi-substituent groups could be confined to construct C_{sp^2}-linked 2D conjugated nanostructures on the metal surface.

Xu et al. synthesized C_{sp^2}-linked 2D conjugated porous polymers using Co (II) phthalocyanine (CoPc) as a building block via the dehydrogenation coupling reaction (**Figure 16**a).[259] As shown in Figure 16b-1, CoPc showed a well-resolved island structure on the Ag (110) substrate. The HR-STM image of single CoPc in Figure 16b-2 clearly demonstrated that its molecule. After annealing at 680 K to trigger C-H activation of CoPc, a C_{sp^2}-linked 2D polymeric network was successfully formed via aryl–aryl coupling of CoPc (Figure 16b-3,4). This network was distinct from that of the self-assembled precursor, indicating the CoPc structure was joined at specific C_2 sites with C_{sp^2}–C_{sp^2} bonds in a uniform staggered fashion. The selective aryl–aryl coupling at the C_2 sites had four structural motifs, leading to a disordered 2D conjugated polymeric network. The dehydrogenation coupling reaction of CoPc on other metal substrates (e.g., Au (111), Cu (100) and Cu (110)) revealed a 2D conjugated polymeric network; however, networks with less regularity were also found on these surfaces. Chi et al. reported the preparation of various 2D conjugated polymeric networks (Figure 16c and e) from 1,3,5-tris(4-hydroxyphenyl)benzene (THPB) and 4,4’’’-dihydroxy-*p*-quaterphenyl (DHQP) via a regioselective aromatic C-H activation reaction using a hydroxyl group as the guiding group.[260] THPB molecules could be self-assembled into well-ordered structures on both gold and silver surfaces. After annealing at 340 °C, two-dimensional polyphenylene frameworks

formed via diselective ortho C-H activation on Au (111) (Figure 16d-1,2), which could be attributed to the successive breaking of the ortho C-H bonds. In contrast, irregular porous networks were obtained on the Ag (111) surface at 300 °C (Figure 16d-3). In the STM images shown in Figure 16d-4, a shoulder–shoulder joined THPB structure can be observed, which indicated monoselective ortho C-H activation on Ag (111). Similar to THPB, the DHQPs formed 2D and 1D conjugated polymeric networks on the surface of Au (111) and Ag (111), respectively (Figure 16f). The controlled diselective ortho C-H activation and monoselective ortho C-H activation were caused by the different energy barriers for dehydrogenation with different metals. The structures of the conjugated polymeric networks were well characterized via XPS measurement.

4.4 On-surface 18e-cyclization reaction

Covalent polymerization on a surface was easily restricted to one-dimensional growth because of the irreversible formation of covalent bonds. Therefore, the surface-assisted construction of rigid building blocks with two-dimensional growth has received increasing attention. However, the formation of benzene from the cyclotrimerization reaction often suffers from the presence of non-planar asymmetric 1,2,4-trisubstituted benzene rings. This leads to the uncontrolled formation of 2D polymeric networks. Compared with the cyclotrimerization reaction, the formation of phthalocyanine with a larger rigid structure is rather attractive. Abel et al. reported the synthesis of a 2D-conjugated organometallic sheet with 18e-cyclization of phthalocyanine on the metal surface via co-evaporation of Fe and 1,2,4,5-tetracyanobenzene (TCNB) under UHV conditions.[261] At room temperature, a contamination-free C_{sp^2}–linked 2D conjugated phthalocyanine film formed on Au (111) and Ag (111), with a TCNB to iron atom stoichiometry of 2:1 (**Figure 17**a). As shown in Figure 17b, the polymeric film network had a square structure with a size of ~10-30 nm. HR-STM (Figure 17c) showed a measured periodicity of 1.15 ± 0.1 nm in two directions, indicating the covalent nature of the C_{sp^2}–C_{sp^2} bonds in the film, which

was consistent with the DFT calculation results. When an insulating film of NaCl/Ag (100) was used as the substrate, the defect-free organometallic sheet with a square structure covered the NaCl island. This approach opens a new avenue for the construction of various electric devices via soft lithography of organic semiconductive films transferred from the insulating NaCl film to other substrates

5. Conclusions

Because of their exclusive physical and chemical properties, 2D porous polymers with sp^2–carbon-based connections and fully sp^2-bonded carbon skeletons hold potential for breakthrough innovation in numerous technologically relevant areas: electronics, catalysis, membrane technology, sensing as well as energy storage and conversion. In a nutshell, bottom-up fabricated 2D porous polymers can be produced as freestanding sheets with tailored properties. Although the "rise of graphene" triggered an intensive research endeavour on 2D materials, this area is still underdeveloped compared to 1D and 3D architectures. Taking advantage of new and improved synthetic methodologies that are continuously emerging, more sophisticated tools are becoming available for the preparation of 2D porous polymers with precisely defined chemical composition and structure leading to novel and outstanding material's properties. However, the development of such 2D porous polymers remains a substantial challenge because of the poor balance between the 2D morphology and C_{sp^2}–C_{sp^2} connections. In addition, the formation of poorly reversible C_{sp^2}–C_{sp^2} bonds is usually detrimental to the formation of a 2D morphology with conjugated polymers. As summarized in this review, several reactions have been used to synthesis 2D conjugated porous polymers or conjugated porous polymer nanosheets, including Gilch raction, Mizoroki–Heck, Suzuki–Miyaura and Yamamoto coupling reactions, Knoevenagel, Aldol condensation reaction, oxidative polymerization reaction, S-replacing reaction, thermally initiated endogenous polymerization reaction, photoinduced polymerization reaction, Ullmann coupling reaction,

cyclotrimerization reaction, dehydrogenative reaction and on-surface 18e-cyclization reaction. In each case, only limited 2DPPs were reported to date via controlled design of the building blocks and optimizing the reaction conditions for confined formation of C_{sp^2}–C_{sp^2} bonds for 2D directional growth. Because of their 2D morphology and conjugated framework, many practical applications of as-developed 2DPPs with C_{sp^2}–C_{sp^2} connections have been demonstrated in the fields of optoelectronics and energy storage and conversion, especially as electrodes for batteries and supercapacitors, precursors for porous carbon-based electrocatalysts, membranes for gas separation, and probes for solid luminescence. Enhancing the structural complexity could generate multifunctional C_{sp^2}-linked 2DPPs with specific properties for a range of applications. Very recently, none-6-membered C_{sp^2} rings, e.g., 4-, 5-, 7-, 8-membered rings, based 2D structures are emerging as new stars of this field.[262]

While C_{sp^2}-linked 2DPPs are a fascinating class of porous materials, the progress of their design and synthesis and exploration of their functionalities is insufficient compared with many other types of 2D soft nanomaterials. To resolve some urgent issues, several improvements need to be considered: (1) Searching for new synthetic methodologies to construct C_{sp^2}-linked 2DPPs with controlled morphologies. For example, the design of rigid building blocks is key for the preparation of C_{sp^2}-linked 2DPPs, except tetraphenylethylene and porphyrin. In addition, new dynamic covalent C_{sp^2}–C_{sp^2} bonds need to be explored for olefin-linked 2D-conjugated COF. (2) The exfoliation of such 2DPPs could produce ultrathin 2D polymers with atomic layer thickness and a large horizontal area. (3) Development of C_{sp^2}-linked 2DPPs with unique optical/electrical properties is highly desirable for environmental and energy application. If these challenges can be met, C_{sp^2}-linked 2DPPs will become increasingly attractive for research and practical application in the future.

Acknowledgements

J.K. and S.H. equally contributed to this work. This work was financially supported by National Key Research and Development Program of China (2017YFE9134000/ T7ΔKI-00039), NSFC Excellent Young Scientists Fund (51722304), NSFC (51973114, 21720102002, 51811530013), Shanghai Pujiang Talent Program (18PJ1406100), Science and Technology Commission of Shanghai Municipality (17ZR1441700, 19JC412600).

Conflict of Interest

The authors declare no conflict of interest.

Received: ((will be filled in by the editorial staff))
Revised: ((will be filled in by the editorial staff))
Published online: ((will be filled in by the editorial staff))

References

[1] M. E. Davis, *Nature* **2002**, 417, 813-821.

[2] J. Germain, J. M. J. Fréchet and F. Svec, *Small* **2009**, 5, 1098-1111.

[3] J. R. Holst and A. I. Cooper, *Adv. Mater.* **2010**, 22, 5212-5216.

[4] A. G. Slater and A. I. Cooper, *Science* **2015**, 348, aaa8075.

[5] A. Thomas, P. Kuhn, J. Weber, M.-M. Titirici and M. Antonietti, *Macromol. Rapid Commun.* **2009**, 30, 221-236.

[6] D. Wu, F. Xu, B. Sun, R. Fu, H. He and K. Matyjaszewski, *Chem. Rev.* **2012**, 112, 3959-4015.

[7] J. Wu, F. Xu, S. Li, P. Ma, X. Zhang, Q. Liu, R. Fu and D. Wu, *Adv. Mater.* **2019**, 31, 1802922.

[8] N. Yanai, K. Kitayama, Y. Hijikata, H. Sato, R. Matsuda, Y. Kubota, M. Takata, M. Mizuno, T. Uemura and S. Kitagawa, *Nature Mater.* **2011**, 10, 787.

[9] X. Zou, H. Ren and G. Zhu, *Chem. Commun.* **2013**, 49, 3925-3936.

[10] A. P. Côté, A. I. Benin, N. W. Ockwig, M. O'Keeffe, A. J. Matzger and O. M. Yaghi, *Science* **2005**, 310, 1166-1170.

[11] H. Furukawa and O. M. Yaghi, *J. Am. Chem. Soc.* **2009**, 131, 8875-8883.

[12] C. J. Doonan, D. J. Tranchemontagne, T. G. Glover, J. R. Hunt and O. M. Yaghi, *Nat. Chem.* **2010**, 2, 235.

[13] X. Feng, X. Ding and D. Jiang, *Chem. Soc. Rev.* **2012**, 41, 6010-6022.

[14] N. Huang, P. Wang and D. Jiang, *Nat. Rev. Mater.* **2016**, 1, 16068.

[15] C. S. Diercks and O. M. Yaghi, *Science* **2017**, 355. eaal1585.

[16] H. Wang, Z. Zeng, P. Xu, L. Li, G. Zeng, R. Xiao, Z. Tang, D. Huang, L. Tang, C. Lai, D. Jiang, Y. Liu, H. Yi, L. Qin, S. Ye, X. Ren and W. Tang, *Chem. Soc. Rev.* **2019**, 48, 488-516.

[17] L. J. Murray, M. Dincă and J. R. Long, *Chem. Soc. Rev.* **2009**, 38, 1294-1314.

[18] A. H. Chughtai, N. Ahmad, H. A. Younus, A. Laypkov and F. Verpoort, *Chem. Soc. Rev.* **2015**, 44, 6804-6849.

[19] P. Silva, S. M. F. Vilela, J. P. C. Tomé and F. A. Almeida Paz, *Chem. Soc. Rev.* **2015**, 44, 6774-6803.

[20] L. Chen, R. Luque and Y. Li, *Chem. Soc. Rev.* **2017**, 46, 4614-4630.

[21] X. Li, Y. Liu, J. Wang, J. Gascon, J. Li and B. Van Der Bruggen, *Chem. Soc. Rev.* **2017**, 46, 7124-7144.

[22] W. P. Lustig, S. Mukherjee, N. D. Rudd, A. V. Desai, J. Li and S. K. Ghosh, *Chem. Soc. Rev.* **2017**, 46, 3242-3285.

[23] L. Zhu, X. Q. Liu, H. L. Jiang and L. B. Sun, *Chem. Rev.* **2017**, 117, 8129-8176.

[24] J. Li, X. Wang, G. Zhao, C. Chen, Z. Chai, A. Alsaedi, T. Hayat and X. Wang, *Chem. Soc. Rev.* **2018**, 47, 2322-2356.

[25] P. Kuhn, M. Antonietti and A. Thomas, *Angew. Chem. Int. Ed.* **2008**, 47, 3450-3453.

[26] P. Kuhn, A. Forget, D. Su, A. Thomas and M. Antonietti, *J. Am. Chem. Soc.* **2008**, 130, 13333-13337.

[27] P. Kuhn, A. Forget, J. Hartmann, A. Thomas and M. Antonietti, *Adv. Mater.* **2009**, 21, 897.

[28] M. J. Bojdys, J. Jeromenok, A. Thomas and M. Antonietti, *Adv. Mater.* **2010**, 22, 2202-2205.

[29] W. Zhang, C. Li, Y.-P. Yuan, L.-G. Qiu, A.-J. Xie, Y.-H. Shen and J.-F. Zhu, *J. Mater. Chem.* **2010**, 20, 6413-6415.

[30] P. Katekomol, J. Roeser, M. Bojdys, J. Weber and A. Thomas, *Chem. Mater.* **2013**, 25, 1542-1548.

[31] J. Artz, *ChemCatChem* **2018**, 10, 1753-1771.

[32] Y. Zhang and S. Jin, *Polymers* **2018**, 11. 31.

[33] M. Liu, L. Guo, S. Jin and B. Tan, *J. Mater. Chem. A* **2019**, 7, 5153-5172.

[34] J. Liu, P. Lyu, Y. Zhang, P. Nachtigall and Y. Xu, *Adv. Mater.* **2018**, 30, 1705401.

[35] P. Kaur, J. T. Hupp and S. T. Nguyen, *ACS Catal.* **2011**, 1, 819-835.

[36] P. Pandey, O. K. Farha, A. M. Spokoyny, C. A. Mirkin, M. G. Kanatzidis, J. T. Hupp and S. T. Nguyen, *J. Mater. Chem.* **2011**, 21, 1700-1703.

[37] Y. Zhang and S. N. Riduan, *Chem. Soc. Rev.* **2012**, 41, 2083-2094.

[38] S. Qiao, W. Huang, T. Wang, B. Du, X. Chen, A. Hameed and R. Yang, *J. Mater. Chem. A* **2017**, 5, 2981-2986.

[39] W. Wang, M. Zhou and D. Yuan, *J. Mater. Chem. A* **2017**, 5, 1334-1347.

[40] W. Zhang, B. Aguila and S. Ma, *J. Mater. Chem. A* **2017**, 5, 8795-8824.

[41] Y. Zhi, K. Li, H. Xia, M. Xue, Y. Mu and X. Liu, *J. Mater. Chem. A* **2017**, 5, 8697-8704.

[42] S. Kramer, N. R. Bennedsen and S. Kegnæs, *ACS Catal.* **2018**, 8, 6961-6982.

[43] J. Yang, M. Yuan, D. Xu, H. Zhao, Y. Zhu, M. Fan, F. Zhang and Z. Dong, *J. Mater. Chem. A* **2018**, 6, 18242-18251.

[44] Y. Luo, B. Li, W. Wang, K. Wu and B. Tan, *Adv. Mater.* **2012**, 24, 5703-5707.

[45] Y. Tan, Q. Gu, J. A. Kimpton, Q. Li, X. Chen, L. Ouyang, M. Zhu, D. Sun and X. Yu, *J. Mater. Chem. A* **2013**, 1, 10155-10165.

[46] X. Yang, M. Yu, Y. Zhao, C. Zhang, X. Wang and J. X. Jiang, *J. Mater. Chem. A* **2014**, 2, 15139-15145.

[47] S. Yao, X. Yang, M. Yu, Y. Zhang and J. X. Jiang, *J. Mater. Chem. A* **2014**, 2, 8054-8059.

[48] J. H. Zhu, Q. Chen, Z. Y. Sui, L. Pan, J. Yu and B. H. Han, *J. Mater. Chem. A* **2014**, 2, 16181-16189.

[49] J. Zhang, Z. A. Qiao, S. M. Mahurin, X. Jiang, S. H. Chai, H. Lu, K. Nelson and S. Dai, *Angew. Chem. Int. Ed.* **2015**, 54, 4582-4586.

[50] C. H. Lau, X. Mulet, K. Konstas, C. M. Doherty, M. A. Sani, F. Separovic, M. R. Hill and C. D. Wood, *Angew. Chem. Int. Ed.* **2016**, 55, 1998-2001.

[51] J. S. M. Lee, M. E. Briggs, T. Hasell and A. I. Cooper, *Adv. Mater.* **2016**, 28, 9804-9810.

[52] S. Wang, M. Xu, T. Peng, C. Zhang, T. Li, I. Hussain, J. Wang and B. Tan, *Nat. Commun.* **2019**, 10, 676.

[53] T. N. Gao, T. Wang, W. Wu, Y. Liu, Q. Huo, Z. A. Qiao and S. Dai, *Adv. Mater.* **2019**, 31, 1806254.

[54] J.-X. Jiang, F. Su, A. Trewin, C. D. Wood, N. L. Campbell, H. Niu, C. Dickinson, A. Y. Ganin, M. J. Rosseinsky, Y. Z. Khimyak and A. I. Cooper, *Angew. Chem. Int. Ed.* **2007**, 46, 8574-8578.

[55] A. I. Cooper, *Adv. Mater.* **2009**, 21, 1291-1295.

[56] A. Li, R. F. Lu, Y. Wang, X. Wang, K. L. Han and W. Q. Deng, *Angew. Chem. Int. Ed.* **2010**, 49, 3330-3333.

[57] J. X. Jiang, C. Wang, A. Laybourn, T. Hasell, R. Clowes, Y. Z. Khimyak, J. Xiao, S. J. Higgins, D. J. Adams and A. I. Cooper, *Angew. Chem. Int. Ed.* **2011**, 50, 1072-1075.

[58] G. Cheng, T. Hasell, A. Trewin, D. J. Adams and A. I. Cooper, *Angew. Chem. Int. Ed.* **2012**, 51, 12727-12731.

[59] W. E. Lee, Y. J. Jin, L. S. Park and G. Kwak, *Adv. Mater.* **2012**, 24, 5604-5609.

[60] C. Gu, Y. Chen, Z. Zhang, S. Xue, S. Sun, K. Zhang, C. Zhong, H. Zhang, Y. Pan, Y. Lv, Y. Yang, F. Li, S. Zhang, F. Huang and Y. Ma, *Adv. Mater.* **2013**, 25, 3443-3448.

[61] C. Gu, N. Huang, J. Gao, F. Xu, Y. Xu and D. Jiang, *Angew. Chem. Int. Ed.* **2014**, 53, 4850-4855.

[62] Y. Zhang, A. Sigen, Y. Zou, X. Luo, Z. Li, H. Xia, X. Liu and Y. Mu, *J. Mater. Chem. A* **2014**, 2, 13422-13430.

[63] Y. Chen, H. Sun, R. Yang, T. Wang, C. Pei, Z. Xiang, Z. Zhu, W. Liang, A. Li and W. Deng, *J. Mater. Chem. A* **2015**, 3, 87-91.

[64] X. Ding and B. H. Han, *Angew. Chem. Int. Ed.* **2015**, 54, 6536-6539.

[65] C. Gu, N. Huang, Y. Chen, L. Qin, H. Xu, S. Zhang, F. Li, Y. Ma and D. Jiang, *Angew. Chem. Int. Ed.* **2015**, 54, 13594-13598.

[66] B. C. Ma, S. Ghasimi, K. Landfester, F. Vilela and K. A. I. Zhang, *J. Mater. Chem. A* **2015**, 3, 16064-16071.

[67] X. Wang, Y. Zhao, L. Wei, C. Zhang and J. X. Jiang, *J. Mater. Chem. A* **2015**, 3, 21185-21193.

[68] S. Zhang, W. Huang, P. Hu, C. Huang, C. Shang, C. Zhang, R. Yang and G. Cui, *J. Mater. Chem. A* **2015**, 3, 1896-1901.

[69] X. Zhuang, D. Gehrig, N. Forler, H. Liang, M. Wagner, M. R. Hansen, F. Laquai, F. Zhang and X. Feng, *Adv. Mater.* **2015**, 27, 3789-3796.

[70] J. S. M. Lee, T. H. Wu, B. M. Alston, M. E. Briggs, T. Hasell, C. C. Hu and A. I. Cooper, *J. Mater. Chem. A* **2016**, 4, 7665-7673.

[71] L. Wang, Y. Wan, Y. Ding, S. Wu, Y. Zhang, X. Zhang, G. Zhang, Y. Xiong, X. Wu, J. Yang and H. Xu, *Adv. Mater.* **2017**, 29, 1702428.

[72] W. Liu, K. Wang, C. Wang, W. Liu, H. Pan, Y. Xiang, D. Qi and J. Jiang, *J. Mater. Chem. A* **2018**, 6, 22851-22857.

[73] R. Dawson, A. I. Cooper and D. J. Adams, *Prog. Polym. Sci.* **2012**, 37, 530-563.

[74] T. Ben, H. Ren, M. Shengqian, D. Cao, J. Lan, X. Jing, W. Wang, J. Xu, F. Deng, J. M. Simmons, S. Qiu and G. Zhu, *Angew. Chem. Int. Ed.* **2009**, 48, 9457-9460.

[75] K. Konstas, J. W. Taylor, A. W. Thornton, C. M. Doherty, W. X. Lim, T. J. Bastow, D. F. Kennedy, C. D. Wood, B. J. Cox, J. M. Hill, A. J. Hill and M. R. Hill, *Angew. Chem. Int. Ed.* **2012**, 51, 6639-6642.

[76] D. E. Demirocak, M. K. Ram, S. S. Srinivasan, D. Y. Goswami and E. K. Stefanakos, *J. Mater. Chem. A* **2013**, 1, 13800-13806.

[77] H. Ma, H. Ren, X. Zou, F. Sun, Z. Yan, K. Cai, D. Wang and G. Zhu, *J. Mater. Chem. A* **2013**, 1, 752-758.

[78] Y. Yuan, F. Sun, F. Zhang, H. Ren, M. Guo, K. Cai, X. Jing, X. Gao and G. Zhu, *Adv. Mater.* **2013**, 25, 6619-6624.

[79] L. Li, H. Ren, Y. Yuan, G. Yu and G. Zhu, *J. Mater. Chem. A* **2014**, 2, 11091-11098.

[80] S. Meng, H. Ma, L. Jiang, H. Ren and G. Zhu, *J. Mater. Chem. A* **2014**, 2, 14536-14541.

[81] C. H. Lau, K. Konstas, A. W. Thornton, A. C. Y. Liu, S. Mudie, D. F. Kennedy, S. C. Howard, A. J. Hill and M. R. Hill, *Angew. Chem. Int. Ed.* **2015**, 54, 2669-2673.

[82] H. Ma, B. Li, L. Zhang, D. Han and G. Zhu, *J. Mater. Chem. A* **2015**, 3, 19346-19352.

[83] X. Wu, R. Wang, H. Yang, W. Wang, W. Cai and Q. Li, *J. Mater. Chem. A* **2015**, 3, 10724-10729.

[84] Z. Yan, Y. Yuan, Y. Tian, D. Zhang and G. Zhu, *Angew. Chem. Int. Ed.* **2015**, 54, 12733-12737.

[85] Y. Dong, S. Das, L. Zhu, T. Ben and S. Qiu, *J. Mater. Chem. A* **2016**, 4, 18822-18831.

[86] A. A. Barkhordarian and C. J. Kepert, *J. Mater. Chem. A* **2017**, 5, 5612-5618.

[87] Y. Yang, Z. Yan, L. Wang, Q. Meng, Y. Yuan and G. Zhu, *J. Mater. Chem. A* **2018**, 6, 5202-5207.

[88] Y. Yuan, Y. Yang, M. Faheem, X. Zou, X. Ma, Z. Wang, Q. Meng, L. Wang, S. Zhao and G. Zhu, *Adv. Mater.* **2018**, 30, 1800069.

[89] N. B. McKeown and P. M. Budd, *Chem. Soc. Rev.* **2006**, 35, 675-683.

[90] B. S. Ghanem, K. J. Msayib, N. B. McKeown, K. D. M. Harris, Z. Pan, P. M. Budd, A. Butler, J. Selbie, D. Book and A. Walton, *Chem. Commun.* **2007**, 1, 67-69.

[91] A. G. McDermott, P. M. Budd, N. B. McKeown, C. M. Colina and J. Runt, *J. Mater. Chem. A* **2014**, 2, 11742-11752.

[92] E. Madrid, P. Cottis, Y. Rong, A. T. Rogers, J. M. Stone, R. Malpass-Evans, M. Carta, N. B. McKeown and F. Marken, *J. Mater. Chem. A* **2015**, 3, 15849-15853.

[93] S. Yi, X. Ma, I. Pinnau and W. J. Koros, *J. Mater. Chem. A* **2015**, 3, 22794-22806.

[94] P. Zhang, X. Jiang, S. Wan and S. Dai, *J. Mater. Chem. A* **2015**, 3, 6739-6741.

[95] S. E. Doris, A. L. Ward, P. D. Frischmann, L. Li and B. A. Helms, *J. Mater. Chem. A* **2016**, 4, 16946-16952.

[96] Z. Wang, H. Ren, S. Zhang, F. Zhang and J. Jin, *J. Mater. Chem. A* **2017**, 5, 10968-10977.

[97] C. G. Bezzu, M. Carta, M. C. Ferrari, J. C. Jansen, M. Monteleone, E. Esposito, A. Fuoco, K. Hart, T. P. Liyana-Arachchi, C. M. Colina and N. B. McKeown, *J. Mater. Chem. A* **2018**, 6, 10507-10514.

[98] R. Williams, L. A. Burt, E. Esposito, J. C. Jansen, E. Tocci, C. Rizzuto, M. Lanč, M. Carta and N. B. McKeown, *J. Mater. Chem. A* **2018**, 6, 5661-5667.

[99] J. Tian, L. Chen, D.-W. Zhang, Y. Liu and Z.-T. Li, *Chem. Commun.* **2016**, 52, 6351-6362.

[100] J. Tian, Z.-Y. Xu, D.-W. Zhang, H. Wang, S.-H. Xie, D.-W. Xu, Y.- H Ren, H. Wang,Y. Liu and Z.-T. Li, *Nat. Commun.* **2016**, 7, 11580.

[101] D.-W. Zhang, H. Wang, J. Tian, Z.-T. Li and Y. Liu, Natl. *Sci. Rev.* **2017**, 4, 426-436.

[102] A. Chaix, G. Mouchaham, A. Shkurenko, P. Hoang, B. Moosa, P. M. Bhatt, K. Adil, K. N. Salama, M. Eddaoudi and N. M. Khashab, *J. Am. Chem. Soc.* **2018**, 140, 14571-14575.

[103] A. Karmakar, R. Illathvalappil, B. Anothumakkool, A. Sen, P. Samanta, A. V. Desai, S. Kurungot and S. K. Ghosh, *Angew. Chem. Int. Ed.* **2016**, 55, 10667-10671.

[104] S. Cai, H. Shi, Z. Zhang, X. Wang, H. Ma, N. Gan, Q. Wu, Z. Cheng, K. Ling, M. Gu, C. Ma, L. Gu, Z. An and W. Huang, *Angew. Chem. Int. Ed.* **2018**, 57, 4005-4009.

[105] A. Halder, M. Ghosh, A. M. Khayum, S. Bera, M. Addicoat, H. S. Sasmal, S. Karak, S. Kurungot and R. Banerjee, *J. Am. Chem. Soc.* **2018**, 140, 10941-10945.

[106] I. Hisaki, Y. Suzuki, E. Gomez, B. Cohen, N. Tohnai and A. Douhal, *Angew. Chem. Int. Ed.* **2018**, 57, 12650-12655.

[107] Q. Yin, P. Zhao, R. J. Sa, G. C. Chen, L. Ü. Jian, T. F. Liu and R. Cao, *Angew. Chem. Int. Ed.* **2018**, 57, 7691-7696.

[108] R.-B. Lin, Y. He, P. Li, H. Wang, W. Zhou and B. Chen, *Chem. Soc. Rev.* **2019**, 48, 1362-1389.

[109] W. L. Leong and J. J. Vittal, *Chem. Rev.* **2011**, 111, 688-764.

[110] M. Servalli and A. D. Schlüter, *Annu. Rev. Mater. Res.* **2017**, 47, 361-389.

[111] X. Zhuang, Y. Mai, D. Wu, F. Zhang and X. Feng, *Adv. Mater.* **2015**, 27, 403-427.

[112] J. Zhu, C. Yang, C. Lu, F. Zhang, Z. Yuan and X. Zhuang, *Acc. Chem. Res.* **2018**, 51, 3191-3202.

[113] M. Bieri, M. Treier, J. Cai, K. Aït-Mansour, P. Ruffieux, O. Gröning, P. Gröning, M. Kastler, R. Rieger, X. Feng, K. Müllen and R. Fasel, *Chem. Commun.* **2009**, 45, 6919-6921.

[114] J. Sakamoto, J. van Heijst, O. Lukin and A. D. Schlüter, *Angew. Chem. Int. Ed.* **2009**, 48, 1030-1069.

[115] M. Osada and T. Sasaki, *Adv. Mater.* **2012**, 24, 210-228.

[116] A. Patra and U. Scherf, *Chem. Eur. J* **2012**, 18, 10074-10080.

[117] J. W. Colson and W. R. Dichtel, *Nature Chem.* **2013**, 5, 453-465.

[118] P. Jagadesan, G. Eder and P. L. McGrier, *J. Mater. Chem. C* **2017**, 5, 5676-5679.

[119] R. Khatioda, D. Talukdar, B. Saikia, K. K. Bania and B. Sarma, *Catal. Sci. Technol.* **2017**, 7, 3143-3150.

[120] K. Yuan, T. Hu, Y. Xu, R. Graf, L. Shi, M. Forster, T. Pichler, T. Riedl, Y. Chen and U. Scherf, *Mater. Chem. Front.* **2017**, 1, 278-285.

[121] K. S. Novoselov, A. K. Geim, S. V. Morozov, D. Jiang, Y. Zhang, S. V. Dubonos, I. V. Grigorieva and A. A. Firsov, *Science* **2004**, 306, 666-669.

[122] Y. Yang, W. Rigdon, X. Huang and X. Li, *Sci. Rep.* **2013**, 3, 2086.

[123] P. Sozzani, S. Bracco, A. Comotti, R. Simonutti, P. Valsesia, Y. Sakamoto and O. Terasaki, *Nat. Mater.* **2006**, 5, 545-551.

[124] T. Uemura, N. Yanai and S. Kitagawa, *Chem. Soc. Rev.* **2009**, 38, 1228-1236.

[125] W. Zhang, J. Cui, C.-a. Tao, Y. Wu, Z. Li, L. Ma, Y. Wen and G. Li, *Angew. Chem. Int. Ed.* **2009**, 48, 5864-5868.

[126] X. Huang, S. Tang, X. Mu, Y. Dai, G. Chen, Z. Zhou, F. Ruan, Z. Yang and N. Zheng, *Nat. Nanotech.* **2010**, 6, 28.

[127] T. Fujie, *Polym. J.* **2016**, 48, 773.

[128] S. Bi, C. Lu, W. Zhang, F. Qiu and F. Zhang, *J. Energy Chem.* **2018**, 27, 99-116.

[129] S. Yang, X. Feng, L. Wang, K. Tang, J. Maier and K. Müllen, *Angew. Chem. Int. Ed.* **2010**, 49, 4795-4799.

[130] Q. Qu, S. Yang and X. Feng, *Adv. Mater.* **2011**, 23, 5574-5580.

[131] S. Yang, X. Feng and K. Müllen, *Adv. Mater.* **2011**, 23, 3575-3579.

[132] X. Zhuang, F. Zhang, D. Wu, N. Forler, H. Liang, M. Wagner, D. Gehrig, M. R. Hansen, F. Laquai and X. Feng, *Angew. Chem. Int. Ed.* **2013**, 125, 9850-9854.

[133] X. Zhuang, F. Zhang, D. Wu and X. Feng, *Adv. Mater.* **2014**, 26, 3081-3086.

[134] A. Azhar, Y. Li, Z. Cai, M. B. Zakaria, M. K. Masud, M. S. A. Hossain, J. Kim, W. Zhang, J. Na, Y. Yamauchi and M. Hu, *Bull. Chem. Soc. Jpn.* **2019**, 92, 875-904.

[135] J. -D. Xiao and H. -L. Jiang, *Acc. Chem. Res.* **2019**, 52, 356-366.

[136] I. Berlanga, M. L. Ruiz-González, J. M. González-Calbet, J. L. G. Fierro, R. Mas-Ballesté and F. Zamora, *Small* **2011**, 7, 1207-1211.

[137] D. N. Bunck and W. R. Dichtel, *J. Am. Chem. Soc.* **2013**, 135, 14952-14955.

[138] Y. Peng, Y. Li, Y. Ban, H. Jin, W. Jiao, X. Liu and W. Yang, *Science* **2014**, 346, 1356-1359.

[139] J. L. Segura, M. J. Mancheño and F. Zamora, *Chem. Soc. Rev.* **2016**, 45, 5635-5671.

[140] J.-Y. Yue, Y.-P. Mo, S.-Y. Li, W.-L. Dong, T. Chen and D. Wang, *Chem. Sci.* **2017**, 8, 2169-2174.

[141] T. Ma, E. A. Kapustin, S. X. Yin, L. Liang, Z. Zhou, J. Niu, L.-H. Li, Y. Wang, J. Su, J. Li, X. Wang, W. D. Wang, W. Wang, J. Sun and O. M. Yaghi, *Science* **2018**, 361, 48-52.

[142] N. A. A. Zwaneveld, R. Pawlak, M. Abel, D. Catalin, D. Gigmes, D. Bertin and L. Porte, *J. Am. Chem. Soc.* **2008**, 130, 6678-6679.

[143] H. G. Gilch and W. L. Wheelwright, *J. Polym. Sci. Part A: Polym. Chem.* **1966**, 4, 1337-1349.

[144] J. Wiesecke and M. Rehahn, *Angew. Chem. Int. Ed.* **2003**, 42, 567-570.

[145] S. Kuch, N. Vilbrandt and M. Rehahn, *Macromol. Rapid Commun.* **2016**, 37, 820-825.

[146] A.-K. Schönbein, M. Wagner, P. W. M. Blom and J. J. Michels, *Macromolecules* **2017**, 50, 4952-4961.

[147] R. Dawson, F. Su, H. Niu, C. D. Wood, J. T. A. Jones, Y. Z. Khimyak and A. I. Cooper, *Macromolecules* **2008**, 41, 1591-1593.

[148] N. T. S. Phan, M. Van Der Sluys and C. W. Jones, *Adv. Synth. Catal.* **2006**, 348, 609-679.

[149] M. Tsutomu, M. Kunio and O. Atsumu, *Bull. Chem. Soc. Jpn.* **1971**, 44, 581-581.

[150] M. Kunio, M. Tsutomu and O. Atsumu, *Bull. Chem. Soc. Jpn.* **1973**, 46, 1505-1508.

[151] R. F. Heck and J. P. Nolley, *J. Org. Chem.* **1972**, 37, 2320-2322.

[152] R. F. Heck, *Acc. Chem. Res.* **1979**, 12, 146-151.

[153] L. Sun, Z. Liang, J. Yu and R. Xu, *Polym. Chem.* **2013**, 4, 1932-1938.

[154] L. Sun, Y. Zou, Z. Liang, J. Yu and R. Xu, *Polym. Chem.* **2014**, 5, 471-478.

[155] Y. Ye, Y. Yajie, M. Xujiao, M. Qinghao, W. Lili, Z. Shuai and Z. Guangshan, *Adv. Mater.* **2018**, 30, 1706507.

[156] N. Miyaura, K. Yamada and A. Suzuki, *Tetra. Lett.* **1979**, 20, 3437-3440.

[157] N. Miyaura, T. Yanagi and A. Suzuki, *Synthetic Commun.* **1981**, 11, 513-519.

[158] N. Miyaura and A. Suzuki, *Chem. Rev.* **1995**, 95, 2457-2483.

[159] J. Weber and A. Thomas, *J. Am. Chem. Soc.* **2008**, 130, 6334-6335.

[160] Q. Chen, J. X. Wang, F. Yang, D. Zhou, N. Bian, X. J. Zhang, C. G. Yan and B. H. Han, *J. Mater. Chem.* **2011**, 21, 13554-13560.

[161] D. Xiao, Y. Li, L. Liu, B. Wen, Z. Gu, C. Zhang and Y. S. Zhao, *Chem. Commun.* **2012**, 48, 9519-9521.

[162] L. Chen, Y. Honsho, S. Seki and D. Jiang, *J. Am. Chem. Soc.* **2010**, 132, 6742-6748.

[163] X. Wu, H. Li, B. Xu, H. Tong and L. Wang, *Polym. Chem.* **2014**, 5, 4521-4525.

[164] K. V. Rao, S. Mohapatra, C. Kulkarni, T. K. Maji and S. J. George, *J. Mater. Chem.* **2011**, 21, 12958-12963.

[165] K. V. Rao, S. Mohapatra, T. K. Maji and S. J. George, *Chem. Eur. J* **2012**, 18, 4505-4509.

[166] L. Chen, Y. Yang and D. Jiang, *J. Am. Chem. Soc.* **2010**, 132, 9138-9143.

[167] J. Dong, K. Zhang, X. Li, Y. Qian, H. Zhu, D. Yuan, Q.-H. Xu, J. Jiang and D. Zhao, *Nat. Commun.* **2017**, 8, 1142.

[168] J. Dong, X. Li, K. Zhang, Y. Di Yuan, Y. Wang, L. Zhai, G. Liu, D. Yuan, J. Jiang and D. Zhao, *J. Am. Chem. Soc.* **2018**, 140, 4035-4046.

[169] J. Dong, Z. Qiao, Y. Pan, S. B. Peh, Y. D. Yuan, Y. Wang, L. Zhai, H. Yuan, Y. Cheng, H. Liang, B. Liu and D. Zhao, *Chem. Mater.* **2019**, 31, 4897-4912.

[170] Y. Takakazu and Y. Akio, *Chem. Lett.* **1977**, 6, 353-356.

[171] T. Yamamoto, *Prog. Polym. Sci.* **1992**, 17, 1153-1205.

[172] T. Yamamoto, *Bull. Chem. Soc. Jpn.* **1999**, 72, 621-638.

[173] T. Yamamoto, *J. Org. Chem.* **2002**, 653, 195-199.

[174] J. Schmidt, M. Werner and A. Thomas, *Macromolecules* **2009**, 42, 4426-4429.

[175] T. Abbie and C. A. I., *Angew. Chem. Int. Ed.* **2010**, 49, 1533-1535.

[176] R. M. Kassab, K. T. Jackson, O. M. El-Kadri and H. M. El-Kaderi, *Res. Chem. Intermed.* **2011**, 37, 747-757.

[177] X.-S. Wang, J. Liu, J. M. Bonefont, D.-Q. Yuan, P. K. Thallapally and S. Ma, *Chem. Commun.* **2013**, 49, 1533-1535.

[178] J. X. Jiang, A. Trewin, D. J. Adams and A. I. Cooper, *Chem. Sci.* **2011**, 2, 1777-1781.

[179] Y. Xu, L. Chen, Z. Guo, A. Nagai and D. Jiang, *J. Am. Chem. Soc.* **2011**, 133, 17622-17625.

[180] X. Liu, Y. Xu and D. Jiang, *J. Am. Chem. Soc.* **2012**, 134, 8738-8741.

[181] Z. -S. Wu, L. Chen, J. Liu, K. Parvez, H. Liang, J. Shu, H. Sachdev, R. Graf, X. Feng and K. Müllen, *Adv. Mater.* **2014**, 26, 1450-1455.

[182] Z. Xiang, Y. Xue, D. Cao, L. Huang, J.-F. Chen and L. Dai, *Angew. Chem. Int. Ed.* **2014**, 53, 2433-2437.

[183] Z. Xiang, D. Cao, L. Huang, J. Shui, M. Wang and L. Dai, *Adv. Mater.* **2014**, 26, 3315-3320.

[184] Z. Xiang and D. Cao, *Macromol. Rapid Commun.* **2012**, 33, 1184-1190.

[185] J. R. Harjani, S. J. Nara and M. M. Salunkhe, *Tetra. Lett.* **2002**, 43, 1127-1130.

[186] Y. Wei, W. Chen, X. Zhao, S. Ding, S. Han and L. Chen, *Polym. Chem.* **2016**, 7, 3983-3988.

[187] A. Yassin, M. Trunk, F. Czerny, P. Fayon, A. Trewin, J. Schmidt and A. Thomas, *Adv. Funct. Mater.* **2017**, 27, 1700233.

[188] S. Bi, Z.-A. Lan, S. Paasch, W. Zhang, Y. He, C. Zhang, F. Liu, D. Wu, X. Zhuang, E. Brunner, X. Wang and F. Zhang, *Adv. Funct. Mater.* **2017**, 27, 1703146.

[189] X. Zhuang, W. Zhao, F. Zhang, Y. Cao, F. Liu, S. Bi and X. Feng, *Polym. Chem.* **2016**, 7, 4176-4181.

[190] E. Jin, M. Asada, Q. Xu, S. Dalapati, M. A. Addicoat, M. A. Brady, H. Xu, T. Nakamura, T. Heine, Q. Chen and D. Jiang, *Science* **2017**, 357, 673-676.

[191] E. Jin, J. Li, K. Geng, Q. Jiang, H. Xu, Q. Xu and D. Jiang, *Nature commun.* **2018**, 9, 4143-4143.

[192] E. Jin, Z. Lan, Q. Jiang, K. Geng, G. Li, X. Wang and D. Jiang, *Chem* **2019**, 5, 1-16.

[193] Y. Zhao, H. Liu, C. Wu, Z. Zhang, Q. Pan, F. Hu, R. Wang, P. Li, X. Huang and Z. Li, *Angew. Chem. Int. Ed.* **2019**, 58, 5376-5381.

[194] S. Xu, G. Wang, B. P. Biswal, M. Addicoat, S. Paasch, W. Sheng, X. Zhuang, E. Brunner, T. Heine, R. Berger and X. Feng, *Angew. Chem. Int. Ed.* **2019**, 58, 849-853.

[195] R. Chen, J.-L. Shi, Y. Ma, G. Lin, X. Lang and C. Wang, *Angew. Chem. Int. Ed.* **2019**, 58, 6430-6434.

[196] S. Bi, C. Yang, W. Zhang, J. Xu, L. Liu, D. Wu, X. Wang, Y. Han, Q. Liang and F. Zhang, *Nat. Commun.* **2019**, 10, 2467.

[197] J. Xu, Y. He, S. Bi, M. Wang, P. Yang, D. Wu, J. Wang and F. Zhang, *Angew. Chem. Int. Ed.* **2019**, 58, 12065-12069.

[198] W.-R. Cui, C.-R. Zhang, W. Jiang, F.-F. Li, R.-P. Liang, J. Liu and J.-D. Qiu, *Nat. Commun.* **2020**, 11, 436.

[199] Y. Z. Cui, Q. Fang, H. Lei, G. Xue and W. T. Yu, *Chem. Phys. Lett.* **2003**, 377, 507-511.

[200] H. Meier, Hans C. Holst and A. Oehlhof, *Eur. J. Org. Chem.* **2003**, 2003, 4173-4180.

[201] N. Xu, R.-L. Wang, D.-P. Li, Z.-Y. Zhou, T. Zhang, Y.-Z. Xie and Z.-M. Su, *New J. Chem.* **2018**, 42, 13367-13374.

[202] H. Lyu, C. S. Diercks, C. Zhu and O. M. Yaghi, *J. Am. Chem. Soc.* **2019**, 141, 6848-6852.

[203] S. Wei, F. Zhang, W. Zhang, P. Qiang, K. Yu, X. Fu, D. Wu, S. Bi and F. Zhang, *J. Am. Chem. Soc.* **2019**, 141, 14272-14279.

[204] J. Schmidt, J. Weber, J. D. Epping, M. Antonietti and A. Thomas, *Adv. Mater.* **2009**, 21, 702-705.

[205] S. Yuan, S. Kirklin, B. Dorney, D.-J. Liu and L. Yu, *Macromolecules* **2009**, 42, 1554-1559.

[206] J. Xia, S. Yuan, Z. Wang, S. Kirklin, B. Dorney, D.-J. Liu and L. Yu, *Macromolecules* **2010**, 43, 3325-3330.

[207] H. Bildirir, I. Osken, T. Ozturk and A. Thomas, *Chem. Eur. J.* **2015**, 21, 9306-9311.

[208] Q. Chen, D.-P. Liu, M. Luo, L.-J. Feng, Y.-C. Zhao and B.-H. Han, *Small* **2014**, 10, 308-315.

[209] H. Yang, S. Zhang, L. Han, Z. Zhang, Z. Xue, J. Gao, Y. Li, C. Huang, Y. Yi, H. Liu and Y. Li, *ACS Appl. Mater. Interfaces* **2016**, 8, 5366-5375.

[210] Y. Zhang, X. Zhuang, Y. Su, F. Zhang and X. Feng, *J. Mater. Chem. A* **2014**, 2, 7742.

[211] L. Wang, S. Sun, Y. He, N. He, F. Zhang, Y. Yao, B. Zhang, X. Zhuang and Y. Chen, *Eur. Polym. J.* **2018**, 98, 125-136.

[212] Y. Su, Z. Yao, F. Zhang, H. Wang, Z. Mics, E. Cánovas, M. Bonn, X. Zhuang and X. Feng, *Adv. Funct. Mater.* **2016**, 26, 5893-5902.

[213] K. Liu, H. Qi, R. Dong, R. Shivhare, M. Addicoat, T. Zhang, H. Sahabudeen, T. Heine, S. Mannsfeld, U. Kaiser, Z. Zheng and X. Feng, *Nat Chem.* **2019**, 11, 994-1000.

[214] T. Zhang, H. Qi, Z. Liao, Y. D. Horev, L. A. Panes-Ruiz, P. S. Petkov, Z. Zhang, R. Shivhare, P. Zhang, K. Liu, V. Bezugly, S. Liu, Z. Zheng, S. Mannsfeld, T. Heine, G. Cuniberti, H. Haick, E. Zschech, U. Kaiser, R. Dong and X. Feng, *Nat. Commun.* **2019**, 10, 4225.

[215] K. Ariga, M. Matsumoto, T. Mori and L. K. Shrestha, *Beilstein J. Nanotechnol.* **2019**, 10, 1559-1587.

[216] A. Azhar, M. B. Zakaria, J. Kim, J. Na, Y. V. Kaneti, A. Fatehmulla, A. M. Aldhafiri, W. A. Farooq, Y. Bando, Y. Yamauchi and J. Lin, *Bull. Chem. Soc. Jpn.* **2019**, 92, 1263-1267.

[217] D. Zhou, X. Tan, H. Wu, L. Tian and M. Li, *Angew. Chem. Int. Ed.* **2019**, 131, 1390-1395.

[218] W. Liu and K. P. Loh, *Acc. Chem. Res.* **2017**, 50, 522-526.

[219] W. Liu, X. Luo, Y. Bao, Y. P. Liu, G.-H. Ning, I. Abdelwahab, L. Li, C. T. Nai, Z. G. Hu, D. Zhao, B. Liu, S. Y. Quek and K. P. Loh, *Nat. Chem.* **2017**, 9, 563-570.

[220] W. Liu, M. Ulaganathan, I. Abdelwahab, X. Luo, Z. Chen, S. J. Rong Tan, X. Wang, Y. Liu, D. Geng, Y. Bao, J. Chen and K. P. Loh, *ACS Nano* **2018**, 12, 852-860.

[221] H. Bouas-Laurent, A. Castellan, J. P. Desvergne and R. Lapouyade, *Chem. Soc. Rev.* **2000**, 29, 43-55.

[222] R. Giménez, M. Piñol and J. L. Serrano, *Chem. Mater.* **2004**, 16, 1377-1383.

[223] P. Kissel, R. Erni, W. B. Schweizer, M. D. Rossell, B. T. King, T. Bauer, S. Götzinger, A. D. Schlüter and J. Sakamoto, *Nat. Chem.* **2012**, 4, 287.

[224] M. Li, A. D. Schlüter and J. Sakamoto, *J. Am. Chem. Soc.* **2012**, 134, 11721-11725.

[225] R. Bhola, P. Payamyar, D. J. Murray, B. Kumar, A. J. Teator, M. U. Schmidt, S. M. Hammer, A. Saha, J. Sakamoto, A. D. Schlüter and B. T. King, *J. Am. Chem. Soc.* **2013**, 135, 14134-14141.

[226] P. Kissel, D. J. Murray, W. J. Wulftange, V. J. Catalano and B. T. King, *Nature Chem.* **2014**, 6, 774.

[227] M. J. Kory, M. Wörle, T. Weber, P. Payamyar, S. W. van de Poll, J. Dshemuchadse, N. Trapp and A. D. Schlüter, *Nat. Chem.* **2014**, 6, 779.

[228] P. Payamyar, K. Kaja, C. Ruiz-Vargas, A. Stemmer, D. J. Murray, C. J. Johnson, B. T. King, F. Schiffmann, J. VandeVondele, A. Renn, S. Götzinger, P. Ceroni, A. Schütz, L.-T. Lee, Z. Zheng, J. Sakamoto and A. D. Schlüter, *Adv. Mater.* **2014**, 26, 2052-2058.

[229] R. Z. Lange, G. Hofer, T. Weber and A. D. Schlüter, *J. Am. Chem. Soc.* **2017**, 139, 2053-2059.

[230] J. Méndez, M. F. López and J. A. Martín-Gago, *Chem. Soc. Rev.* **2011**, 40, 4578-4590.

[231] X. Zhang, Q. Zeng and C. Wang, *Nanoscale* **2013**, 5, 8269-8287.

[232] L. Dong, P. N. Liu and N. Lin, *Acc. Chem. Res.* **2015**, 48, 2765-2774.

[233] G. Franc and A. Gourdon, *Phys. Chem. Chem. Phys* **2011**, 13, 14283-14292.

[234] F. Ullmann and J. Bielecki, *Berichte der deutschen chemischen Gesellschaft* **1901**, 34, 2174-2185.

[235] F. Ullmann, *Justus Liebigs Annalen der Chemie* **1904**, 332, 38-81.

[236] M. Xi and B. E. Bent, *J. Am. Chem. Soc.* **1993**, 115, 7426-7433.

[237] S. W. Hla, L. Bartels, G. Meyer and K. H. Rieder, *Phys. Rev. Lett.* **2000**, 85, 2777-2780.

[238] C. Sambiagio, S. P. Marsden, A. J. Blacker and P. C. McGowan, *Chem. Soc. Rev.* **2014**, 43, 3525-3550.

[239] S. Mondal, *ChemTexts* **2016**, 2, 17.

[240] C. J. Judd, S. L. Haddow, N. R. Champness and A. Saywell, *Sci. Rep.* **2017**, 7, 14541.

[241] L. Grill, M. Dyer, L. Lafferentz, M. Persson, M. V. Peters and S. Hecht, *Nat. Nanotech.* **2007**, 2, 687-691.

[242] L. Lafferentz, V. Eberhardt, C. Dri, C. Africh, G. Comelli, F. Esch, S. Hecht and L. Grill, *Nat. Chem.* **2012**, 4, 215.

[243] L. Smykalla, P. Shukrynau, M. Korb, H. Lang and M. Hietschold, *Nanoscale* **2015**, 7, 4234-4241.

[244] M. Bieri, M.-T. Nguyen, O. Gröning, J. Cai, M. Treier, K. Aït-Mansour, P. Ruffieux, C. A. Pignedoli, D. Passerone, M. Kastler, K. Müllen and R. Fasel, *J. Am. Chem. Soc.* **2010**, 132, 16669-16676.

[245] L. Cardenas, R. Gutzler, J. Lipton-Duffin, C. Fu, J. L. Brusso, L. E. Dinca, M. Vondráček, Y. Fagot-Revurat, D. Malterre, F. Rosei and D. F. Perepichka, *Chem. Sci.* **2013**, 4, 3263-3268.

[246] R. Gutzler, H. Walch, G. Eder, S. Kloft, W. M. Heckl and M. Lackinger, *Chem. Commun.* **2009**, 29, 4456-4458.

[247] M. O. Blunt, J. C. Russell, N. R. Champness and P. H. Beton, *Chem. Commun.* **2010**, 46, 7157-7159.

[248] C. Morchutt, J. Björk, S. Krotzky, R. Gutzler and K. Kern, *Chem. Commun.* **2015**, 51, 2440-2443.

[249] J. Eichhorn, D. Nieckarz, O. Ochs, D. Samanta, M. Schmittel, P. J. Szabelski and M. Lackinger, *ACS Nano* **2014**, 8, 7880-7889.

[250] M. Fritton, D. A. Duncan, P. S. Deimel, A. Rastgoo-Lahrood, F. Allegretti, J. V. Barth, W. M. Heckl, J. Björk and M. Lackinger, *J. Am. Chem. Soc*. **2019**, 141, 4824-4832.

[251] S. Yuan, B. Dorney, D. White, S. Kirklin, P. Zapol, L. Yu and D.-J. Liu, *Chem. Commun.* **2010**, 46, 4547-4549.

[252] D. L. J. Broere and E. Ruijter, *Synthesis* **2012**, 44, 2639-2672.

[253] J. Eichhorn, W. M. Heckl and M. Lackinger, *Chem. Commun.* **2013**, 49, 2900-2902.

[254] J. Liu, P. Ruffieux, X. Feng, K. Mullen and R. Fasel, *Chem. Commun.* **2014**, 50, 11200-11203.

[255] H. Zhou, J. Liu, S. Du, L. Zhang, G. Li, Y. Zhang, B. Z. Tang and H.-J. Gao, *J. Am. Chem. Soc.* **2014**, 136, 5567-5570.

[256] B. Yang, J. Björk, H. Lin, X. Zhang, H. Zhang, Y. Li, J. Fan, Q. Li and L. Chi, *J. Am. Chem. Soc.* **2015**, 137, 4904-4907.

[257] C.-J. Li, *Acc. Chem. Res.* **2009**, 42, 335-344.

[258] C. J. Scheuermann, *Chem. Asian J.* **2010**, 5, 436-451.

[259] Q. Sun, C. Zhang, L. Cai, L. Xie, Q. Tan and W. Xu, *Chem. Commun.* **2015**, 51, 2836-2839.

[260] Q. Li, B. Yang, H. Lin, N. Aghdassi, K. Miao, J. Zhang, H. Zhang, Y. Li, S. Duhm, J. Fan and L. Chi, *J. Am. Chem. Soc.* **2016**, 138, 2809-2814.

[261] M. Abel, S. Clair, O. Ourdjini, M. Mossoyan and L. Porte, *J. Am. Chem. Soc.* **2011**, 133, 1203-1205.

[262] Q. Fan, D. Martin-Jimenez, D. Ebeling, C. K. Krug, L. Brechmann, C. Kohlmeyer, G. Hilt, W. Hieringer, A. Schirmeisen, J. M. Gottfried, *J. Am. Chem. Soc.* **2019**, 141, 17713-17720.

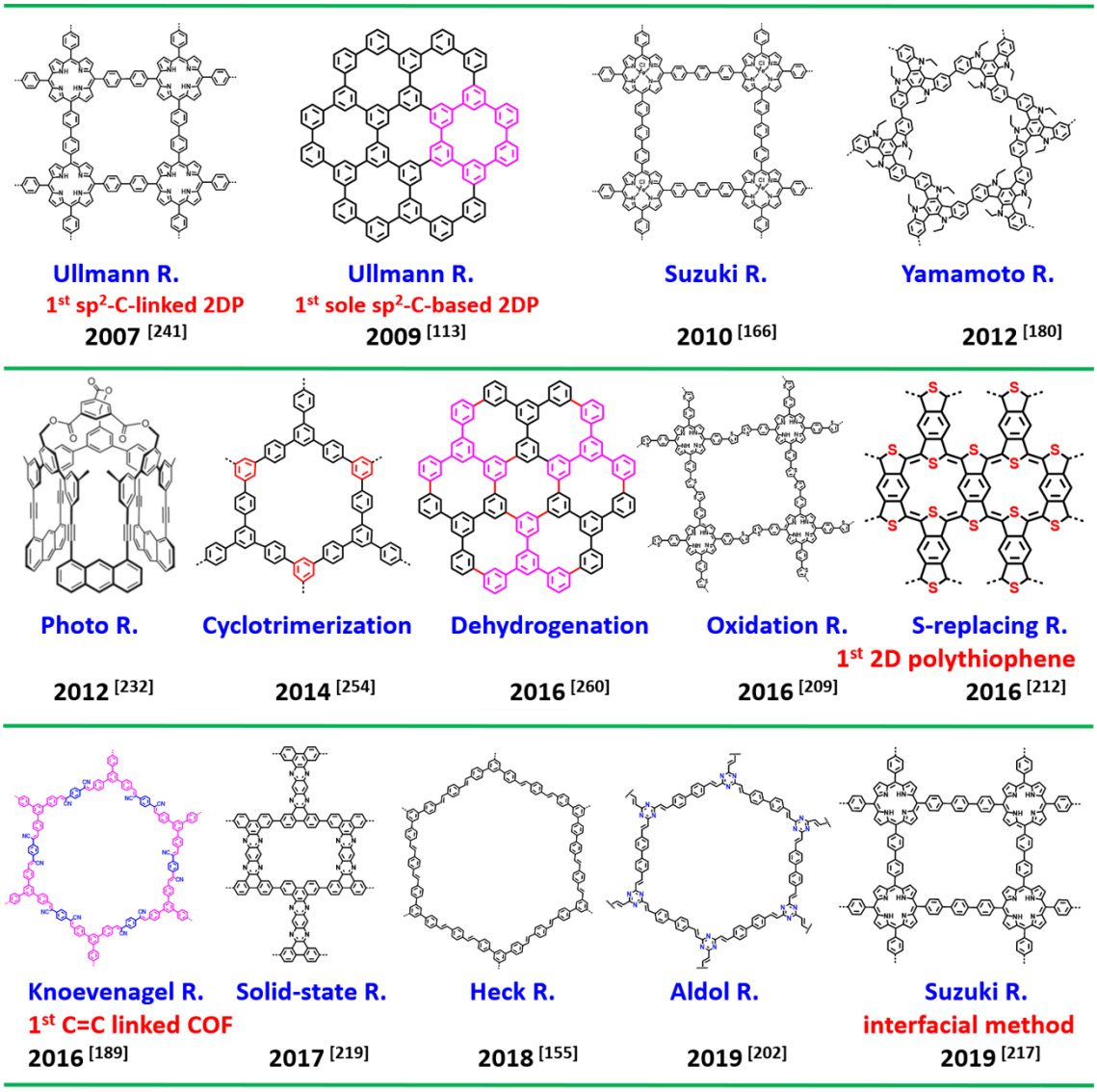

Figure 1. The milestones of the 2D porous polymers with C_{sp^2}–C_{sp^2} connections based on different reactions.

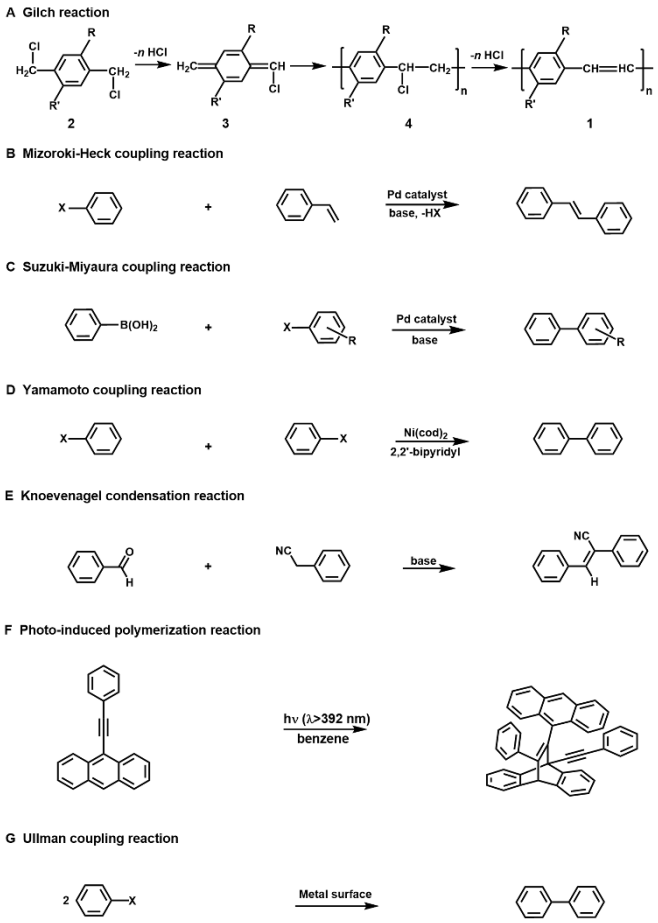

Scheme 1. Model reactions for synthesis of 2D polymers with C_{sp^2}–C_{sp^2} connections.

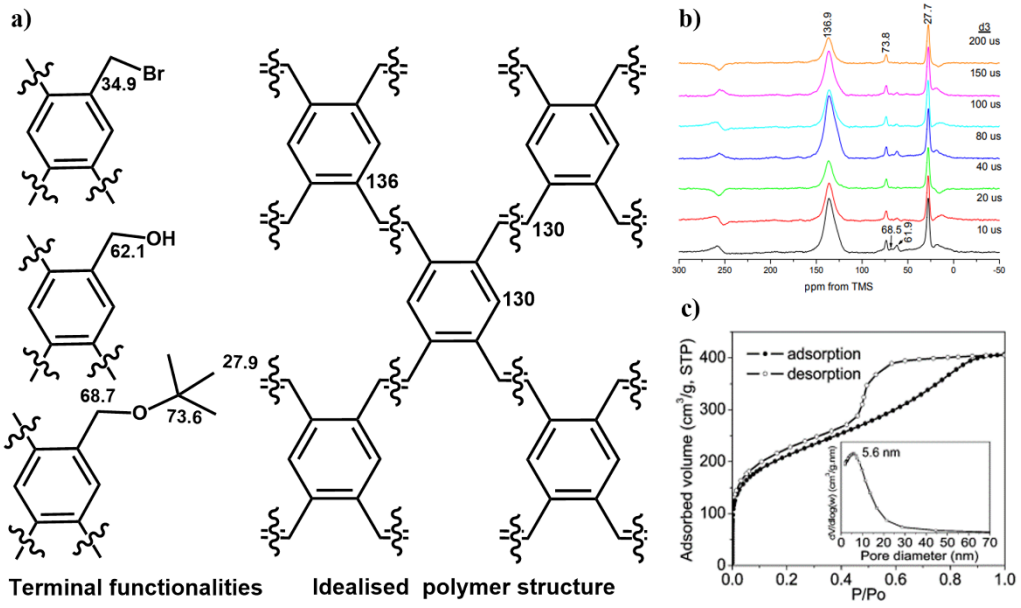

Figure 2. a) Mesoporous PPVs network. b) ^{1}H-^{13}C CP/MAS dipolar dephasing NMR spectra recorded at a MAS rate of 12 kHz and a CP contact time of 2 ms. c) Nitrogen adsorption/desorption isotherms at 77.3 K. Reproduced with permission.[147] Copyright 2008, American Chemical Society.

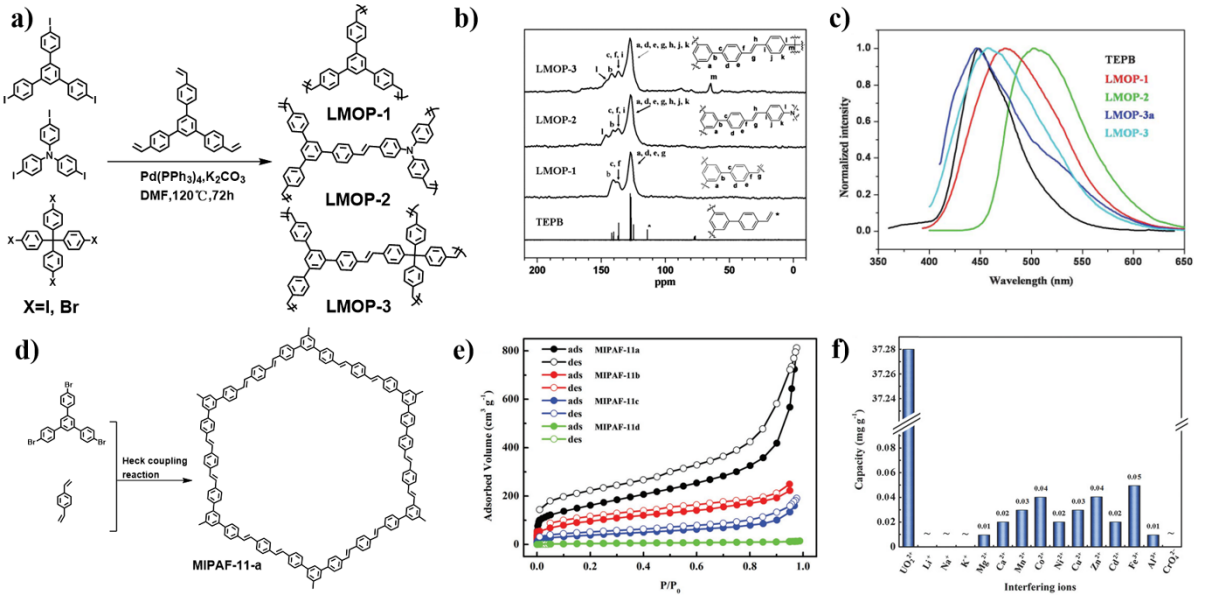

Figure 3. a) Synthesis of LMOPs via the Heck reaction of aromatic halides and 1,3,5-tri(4-ethenylphenyl) benzene. b) ^{13}C CP/MAS NMR spectra of LMOPs (structures of LMOPS are presented in a) and ^{13}C NMR of TEPB. c) Solid state luminescent spectra of TEPB and LMOPs. Reproduced with permission.[153] Copyright 2013, Royal Society of Chemistry. d) Synthetic routes of MIPAF-11-a. e) Nitrogen adsorption isotherms for MIPAFs. f) Ion capacity of MIPAF-11c in the presence of different interfering ions. Reproduced with permission.[155] Copyright 2018, Wiley-VCH.

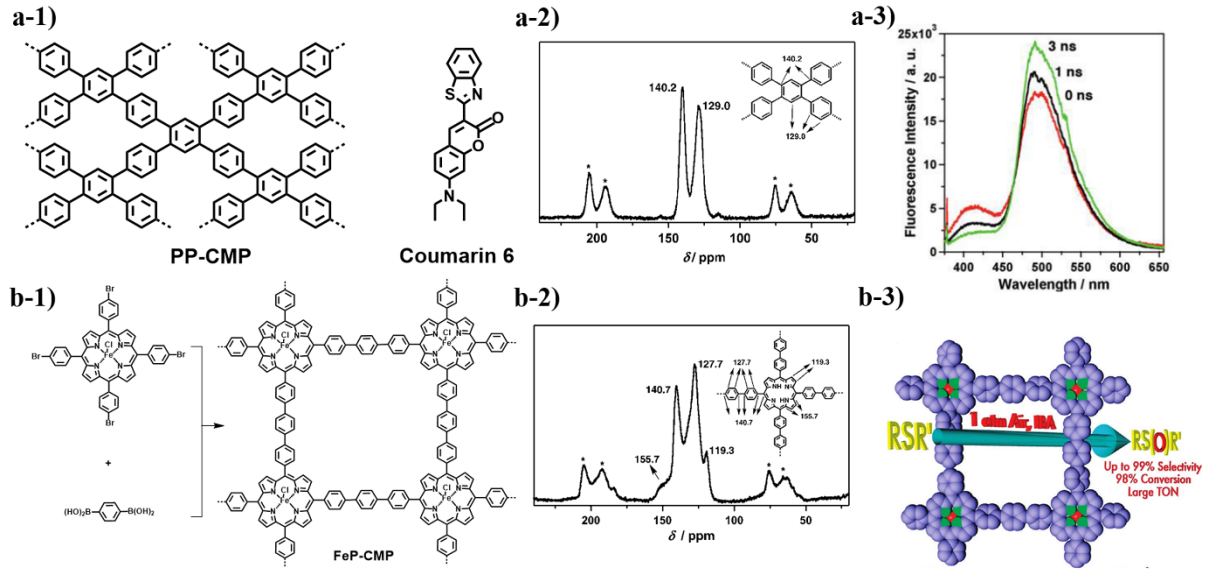

Figure 4. a-1) Structure of PP-CMP and Coumarin 6. a-2) Solid-state ^{1}H-^{13}C CP/MAS NMR spectrum of PP-CMP. a-3) Transient fluorescence spectra of PP-CMP⊃coumarin 6 (coumarin 6 content = 2.9 mol %) observed at 0, 1, and 3 ns after exposure to laser pulse. Reproduced with permission.[162] Copyright 2010, American Chemical Society. b-1) Structure of nanoporous polymer with metalloporphyrin built-in skeleton (FeP-CMP). b-2) Solid-state ^{1}H-^{13}C CP/MAS NMR spectrum of free-base porphyrin CMP. b-3) Transformation of sulfides to sulfoxides catalysed by FeP-CMP. Reproduced with permission.[166] Copyright 2010, American Chemical Society.

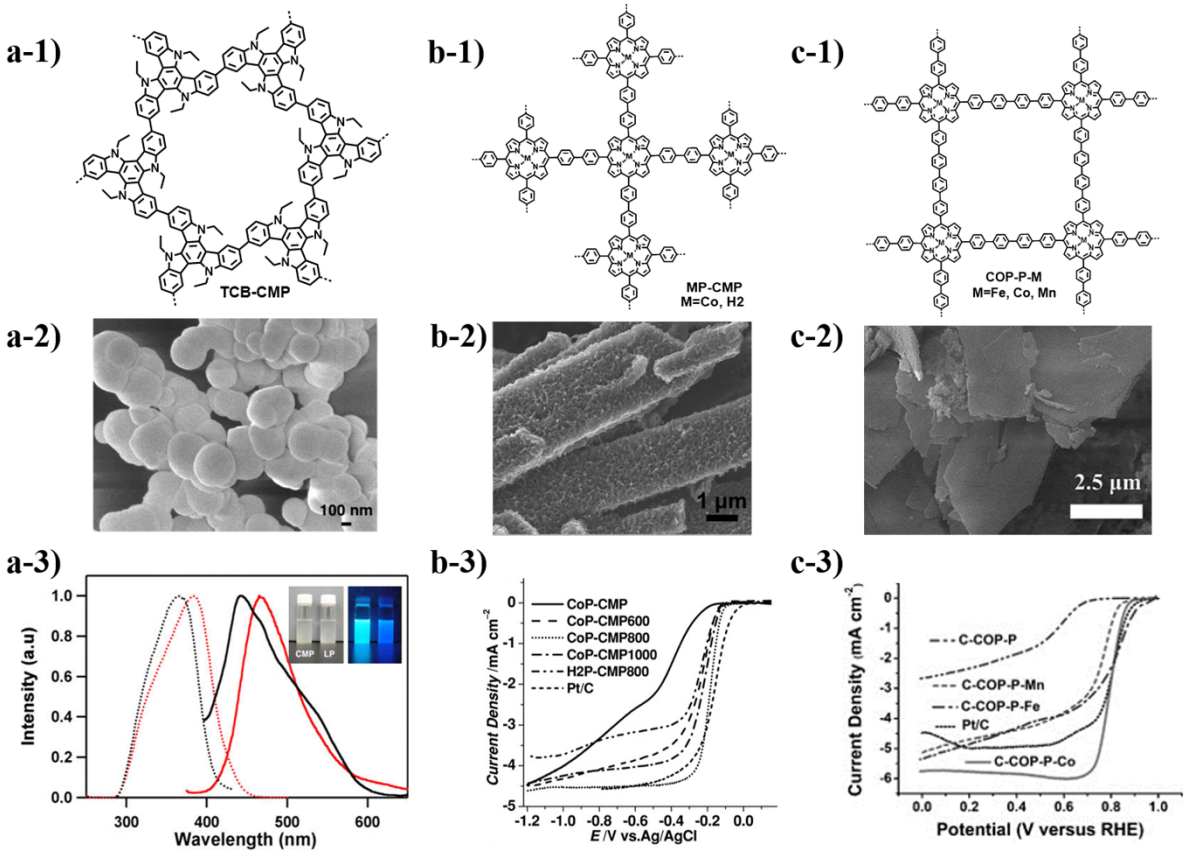

Figure 5. a) Demonstrates the structure a-1) and SEM image a-2) of carbazole-based CMP (TCB-CMP). a-3) UV-vis (dotted curves) and fluorescence spectra (solid curves) of TCB-CMP (red) and CB-LP (black) powders. Reproduced with permission.[180] Copyright 2012, American Chemical Society. b-1) The structure of metalloporphyrin-based conjugated mesoporous polymer frameworks (M = Co, H2). b-2) SEM image of CoP-CMP800. b-3) LSV curves in O_2-saturated 0.1 M KOH at 10 mV s^{-1} at 1600 rpm. Reproduced with permission.[181] Copyright 2013, Wiley-VCH. c-1) COP-P-M (M = Fe, Co, and Mn). c-2) SEM image of COP-P-Fe. c-3) LSV curves of metal-incorporated C-COP-P-M in O_2-saturated 0.1M KOH at 1600 rpm at a sweep rate of 5 mV s^{-1}. Reproduced with permission.[182] Copyright 2014, Wiley-VCH.

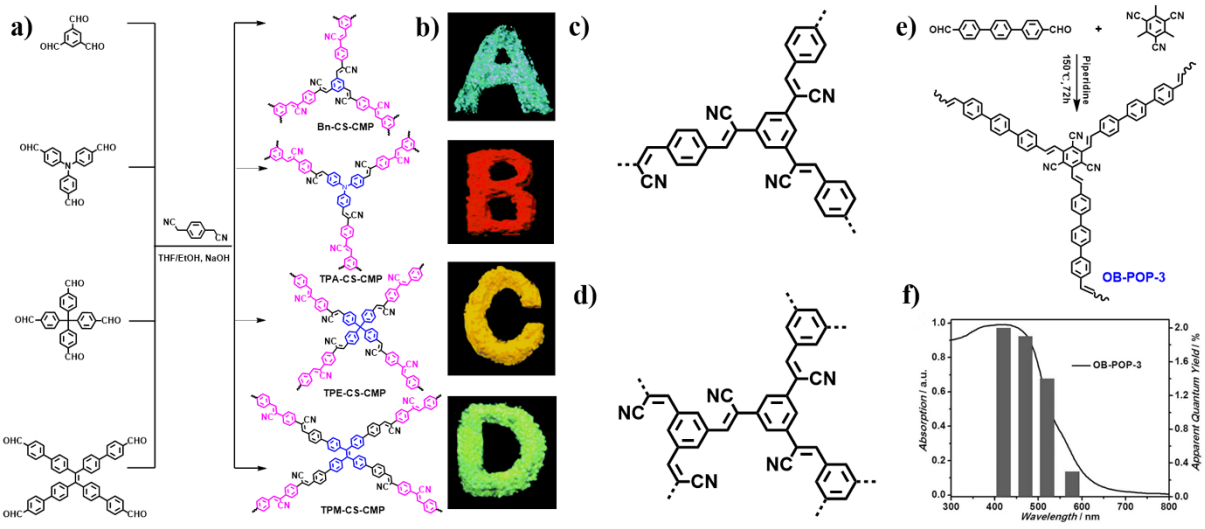

Figure 6. a) Synthetic routes of the four cyanostilbene-based conjugated polymers. b) Photos of Bn-CS-CMP, TPA-CS-CMP, TPE-CS-CMP, and TPM-CS-CMP under illumination of a 365 nm UV lamp. Reproduced with permission.[186] Copyright 2016, Royal Society of Chemistry. c, d) Structure of P5 c) and P6 d). Reproduced with permission.[187] Copyright 2017, Wiley-VCH. e) Synthetic process of olefin-bridged porous organic polymers OB-POP-3. f) Overlay of UV–vis absorption and wavelength-specific AQY on H_2 evolution using Pt-modified OB-POP-3. Reproduced with permission. [188] Copyright 2017, Wiley-VCH.

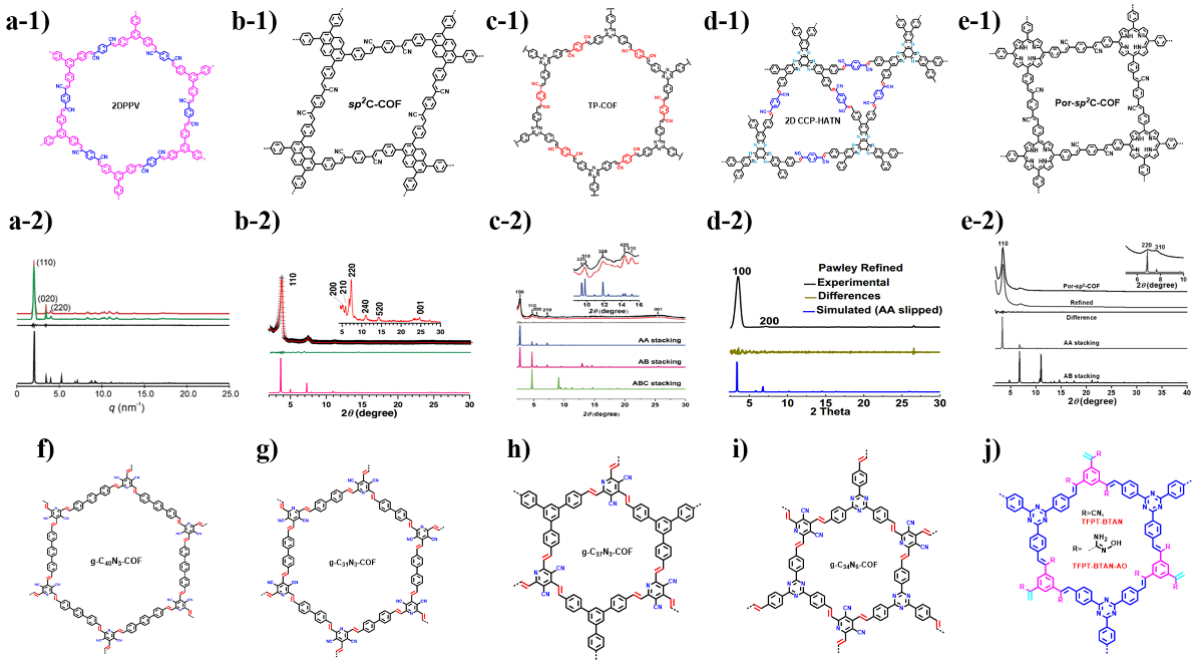

Figure 7. Typical examples of olefin-linked 2D COFs. a-e) The structures (x-1) and PXRD patterns (x-2, x = a, b, c, d, e) of the 1st olefin-linked 2D COF (2DPPV, a-1), the sp^2-hybridized carbon COF (sp^2C-COF, b-1), TP-COF (c), 2D CCP-HATN (d) and Por-sp^2C-COF (e). (a) Reproduced with permission.[189] Copyright 2016, Royal Society of Chemistry. (b). Reproduced with permission from.[190] Copyright 2017, American Association for the Advancement of Science. (c) Reproduced with permission. [193] Copyright 2019, Wiley-VCH. (d) Reproduced with permission.[194] Copyright 2019, Wiley-VCH. (e). Reproduced with permission.[195] Copyright 2019, Wiley-VCH. Six latest olefin-linked 2D COFs: g-$C_{40}N_3$-COF (f), g-$C_{31}N_3$-COF (g), and g-$C_{37}N_3$-COF (h). (f-h) Reproduced with permission.[196] Copyright 2019, Nature Publishing Group. (i) g-$C_{34}N_6$-COF. Reproduced with permission.[197] Copyright 2019, Wiley-VCH. (j) TFPT-BTAN and TFPT-BTAN-AO. Reproduced with permission.[198] Copyright 2020, Nature Publishing Group.

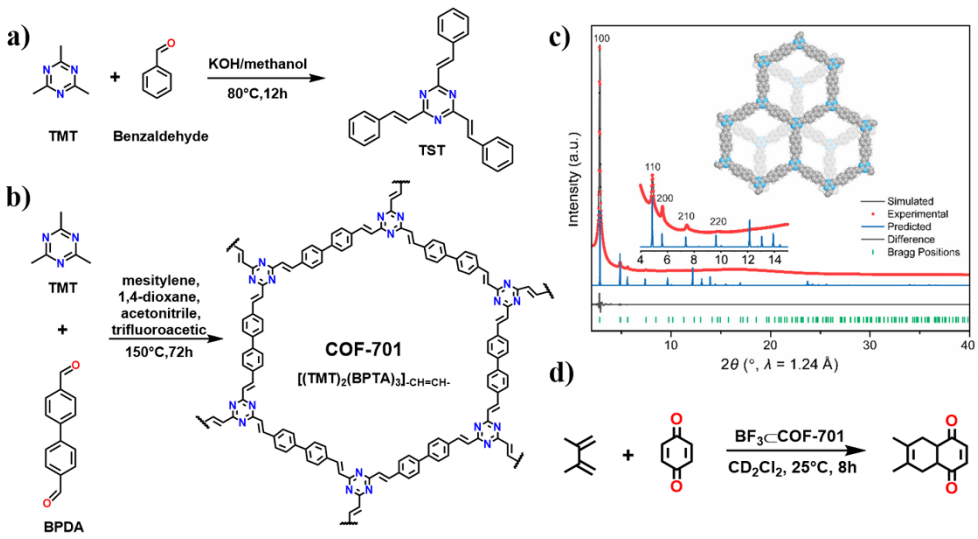

Figure 8. a) Reaction scheme of Aldol condensation between TMT and benzaldehyde to yield the model compound TST. b) Synthesis of COF-701 by aldol condensation between TMT and BPDA. c) Pawley refinement of COF-701 (staggered, AB) against the experimental WAXS pattern. Colour code of the structure model: H, white; C, gray; N, blue. d) Catalytic activity of $BF_3 \subset$COF-701 in a Diels-Alder reaction. Reproduced with permission.[202] Copyright 2019, American Chemical Society.

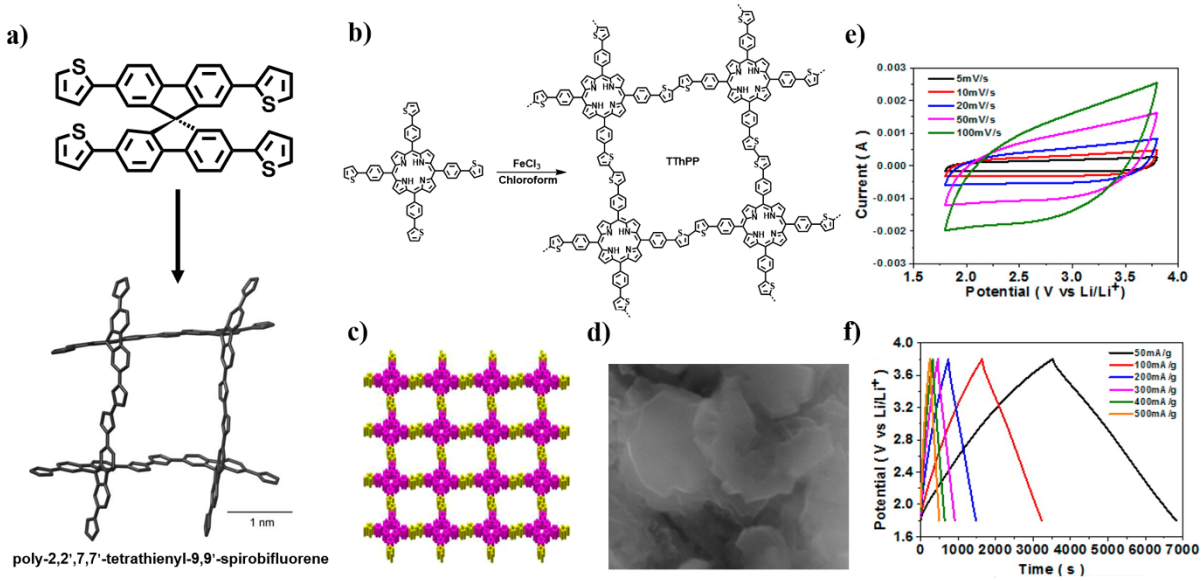

Figure 9. a) Synthesis route of poly-2,2',7,7'-tetrathienyl-9,9'-spirobifluorene. Reproduced with permission.[204] Copyright 2016, Wiley-VCH. Synthesis route b) and c) side view of the model structure of TThPP based on quantum-chemical density functional theory (DFT) calculations (porphyrin: pink, thiophene: yellow; H atoms are omitted for clarity). d) High-magnification SEM image of the TThPP film, e) CV curves of TThPP electrode hybrid capacitors. f) Galvanostatic charge−discharge voltage profiles at various current densities. Reproduced with permission.[209] Copyright 2016, American Chemical Society.

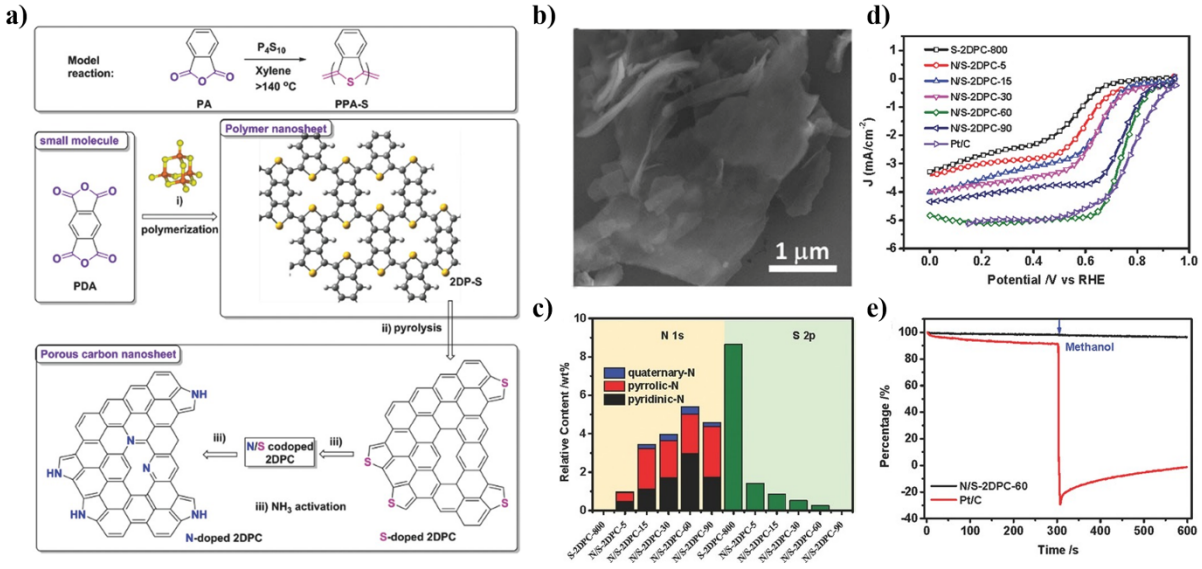

Figure 10. a) Preparation of 2DP-S and 2DPCs. i) Phosphorus pentasulfide, xylene, 140 °C, 3 d; ii) nitrogen, 800 °C, 900 °C, or 1000 °C, 5 °C min^{-1}, 2 h; iii) ammonia gas, 800 °C, 5-90 min. PA: 1,2-benzenedicarboxylic anhydride; PDA: 1,2,4,5-benzenetetracarboxylic anhydride. b)

SEM images of 2DP-S. c) N and S elemental analysis of the N/S-2DPCs based on X-ray photoelectron spectroscopy (XPS) results. d) Rotating disk electrode (RDE) voltammograms of 2DPCs and Pt/C at a rotation rate of 1600 rpm. e) Chronoamperometric responses in O_2-saturated 0.1 M KOH for the N/S-2DPC-60 (black line) and Pt/C (red line) electrocatalysts at 0.65 V, where the arrow indicates the addition of 2% (v/v) methanol. Reproduced with permission.[212] Copyright 2016, Wiley-VCH.

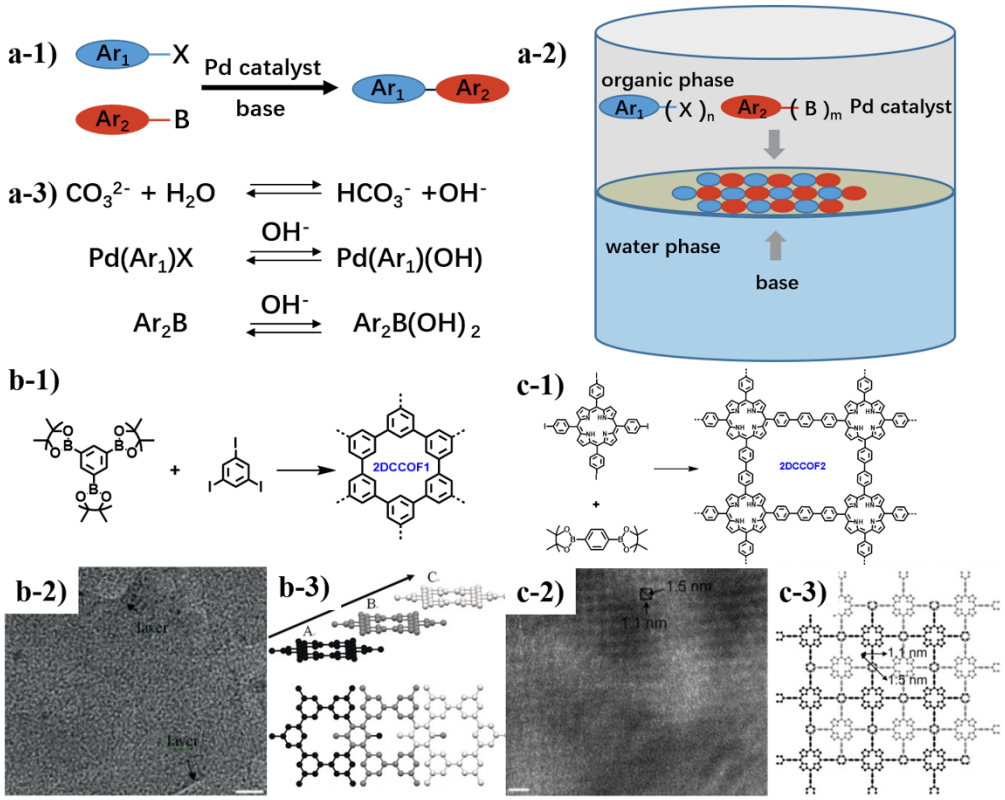

Figure 11. a-1) The model Suzuki reaction between aryl monomers. a-2) Synthesis of 2D-COF on the interface by Suzuki reaction (Ar = aryl group; X = halide; B = boronic group; m, n ≥ 2 and at least one ≥ 3). a-3) Reversible hydroxide/halogen exchange or hydroxylation of boronic group in the transmetalation step (OH^- was generated by the reversible hydrolysis of CO_3^{2-}). Synthetic routes b-1) and HRTEM images b-2) for 2DCCOF1 and 2DCCOF2. b-3) Side view and top view of the A-B-C… stacked structure. c-3) Top view of the proposed structure with AB aggregation. Reproduced with permission.[217] Copyright 2019, Wiley-VCH.

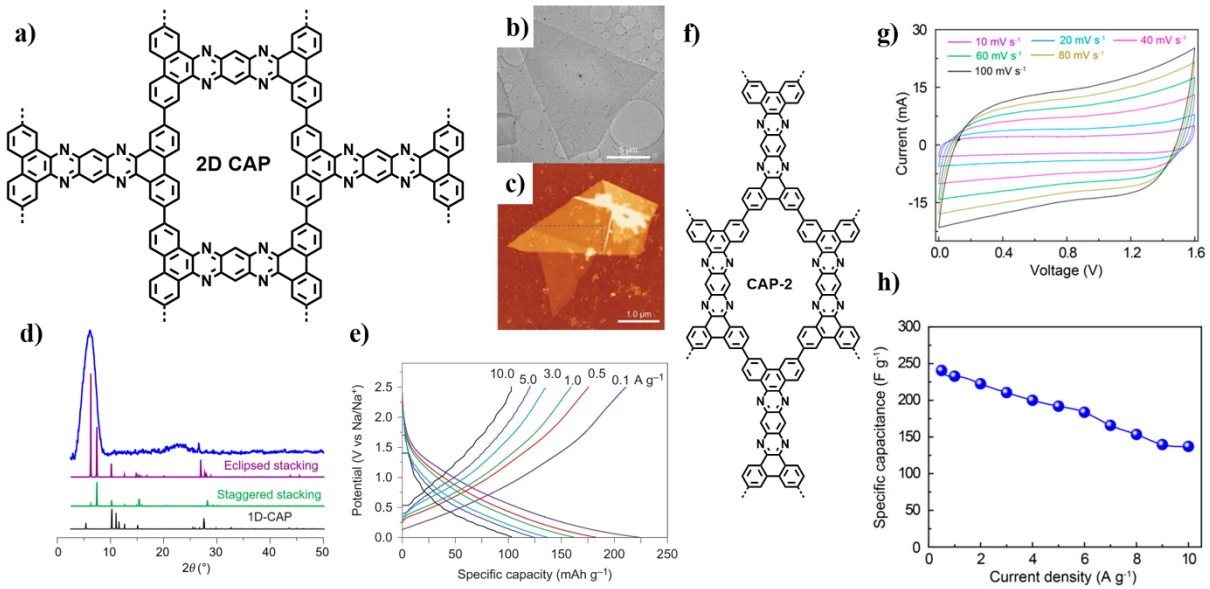

Figure 12. a-e) Structure, characterization and energy storage performance of 2D-CAP: a) Structure, b) TEM image, c) AFM profile, d) XRD pattern and e) Galvanostatic charge–discharge profiles of 2D-CAP. Reproduced with permission. [219] Copyright 2017, Nature Publishing Group. The structure (f), cyclic voltamograms (g) and corresponding specific capacitances of the asymmetric cell (h) of CAP-2. Reproduced with permission.[220] Copyright 2018, American Chemical Society.

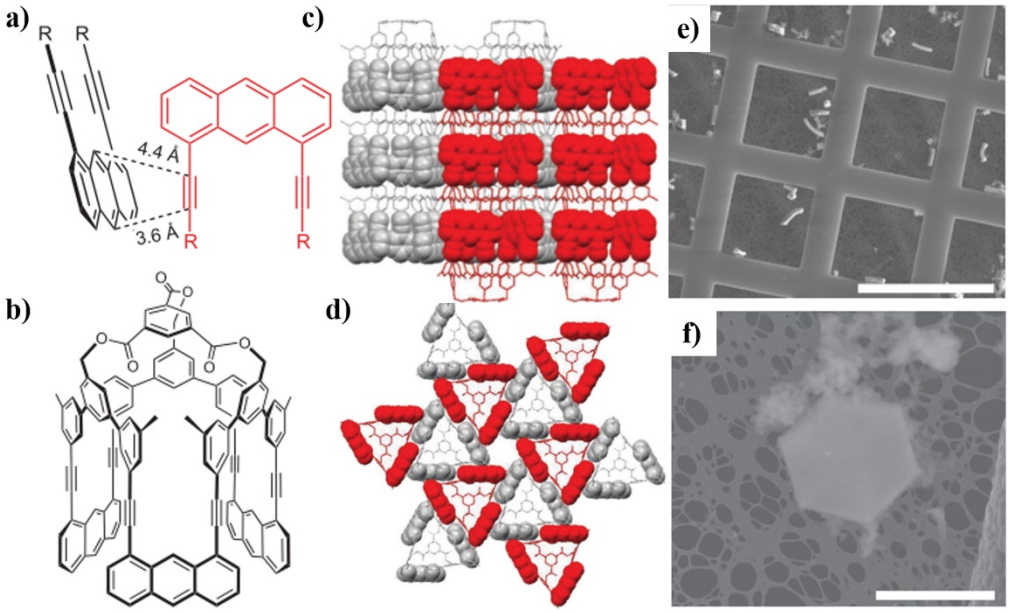

Figure 13. a) The C9,10 anthracene positions of one monomer being opposed to the alkynes of the adjacent monomers at distances of 4.4 and 3.6 Å, respectively. b) Chemical structure of the monomer. c) Laminar crystal structure obtained by XRD with all anthracenes and alkynes displayed as space filling and all other parts as stick models. The monomers oriented up and down are presented in red and gray, respectively. d) Laterally hexagonally packed monomers in each layer. e, f, SEM micrographs of photo-irradiated monomer crystals swollen in an organic solvent. Curved rods e), with a remaining hexagonal cross-section f). Reproduced with permission.[232] Copyright 2012, Nature Publishing Group.

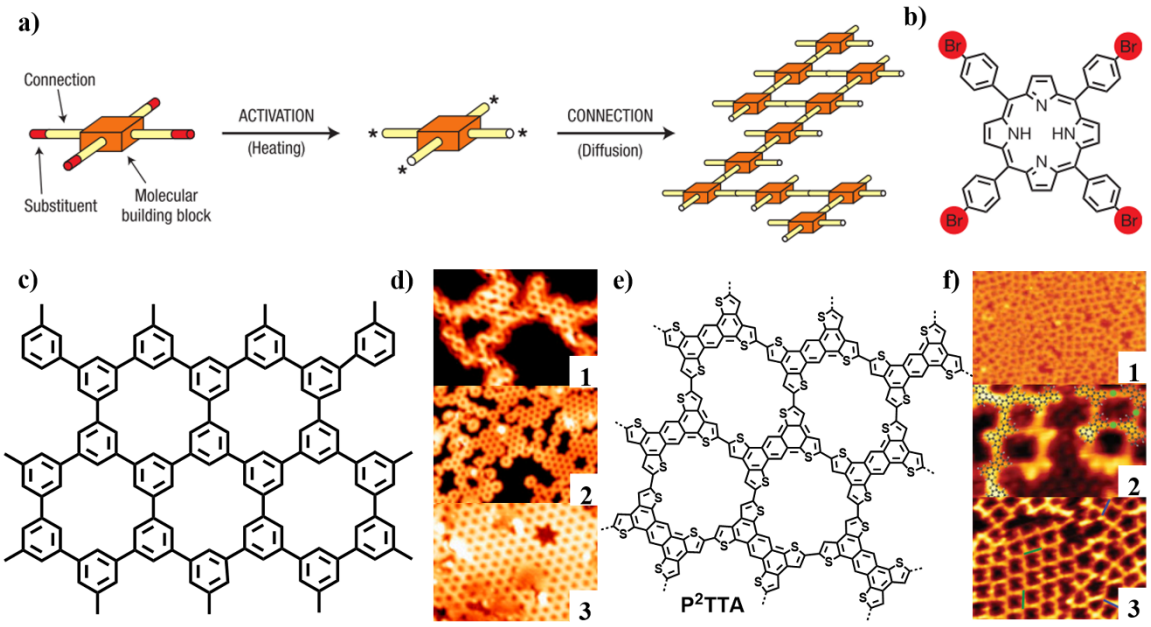

Figure 14. a) Surface formation of 2D porphyrin networks based on C_{sp^2}–C_{sp^2} connections. b) Chemical structure of the Br_4TPP molecule (substituent Br atoms are highlighted in red). Reproduced with permission.[241] Copyright 2007, Nature Publishing Group. c) Chemical structure of a fraction of the polyphenylene network. d) STM images of polyphenylene networks on Cu (111) 1), Au (111) 2), and Ag (111) 3). Reproduced with permission.[244] Copyright 2010, American Chemical Society. e) The structure of the covalent polymer P^2TTA. f) 1. STM image of the P^2TTA polymer on Ag (111) (U = -0.8 V, I = 0.5 nA). 2. Close-up of polymeric (left molecular model) and organometallic (right model) structures; coadsorbed atomic Br is observed in the lower portion of the image in a $\sqrt{3}\times\sqrt{3}$-R30° reconstruction (U= -0.7 V, I = 0.8 nA). 3. STM topography of polymeric and organometallic structures (U= -0.7 V, I = 0.8 nA). Reproduced with permission.[245] Copyright 2013, Royal Society of Chemistry.

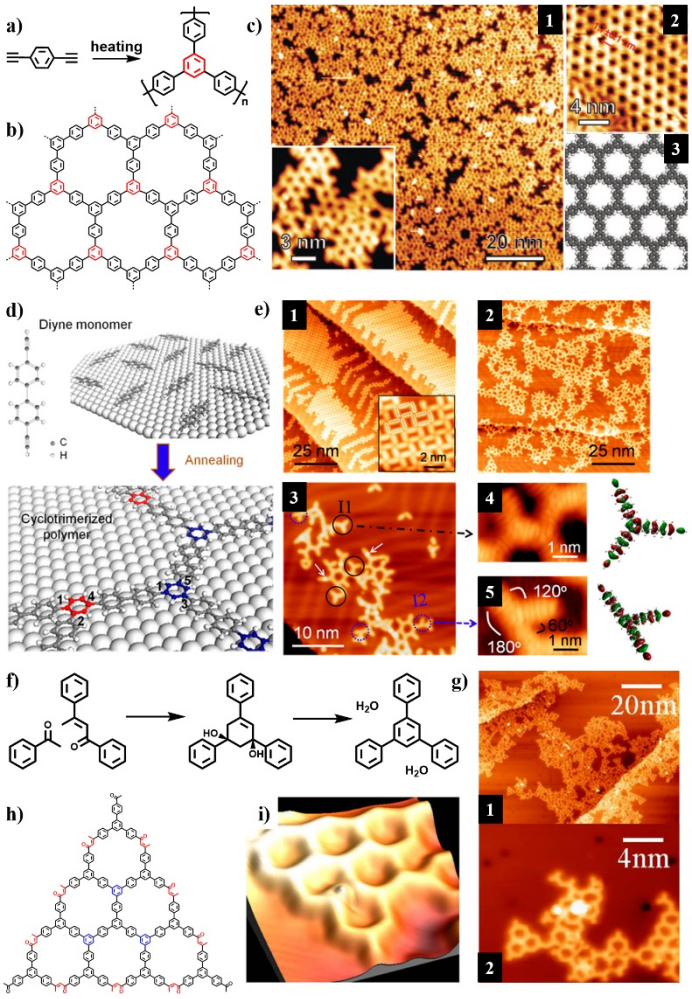

Figure 15. a) Ethynyl cyclotrimerization reaction. b) Chemical structure of a fraction of a 2D polyphenylene network. c-1) Low-magnification STM image of the 2D polymer network obtained by cyclotrimerization of TEB on Au (111) at 160 °C. The inset is a magnified image. c-2) STM image of a regular domain of the 2D honeycomb polymer with the corresponding structural model depicted in c-3). Reproduced with permission.[254] Copyright 2014, Royal Society of Chemistry. d) Experimental procedure and proposed polymeric mechanism. (Upper panel) DEBP monomers were thermally deposited onto the Au (111) surface. (Lower panel) Annealing caused cyclotrimerization of the diyne molecules: three triple bonds were cyclotrimerized into one benzene ring with either 1,3,5- (blue) or 1,2,4- (red) trisubstitution. e) STM images of the molecular layer before and after annealing. e-1) Initial deposition on the Au (111) surface with approximately 0.5 ML coverage. The inset is a magnified image with several molecular models superimposed to guide the eyes. e-2) After annealing at 100 °C, the diyne molecules were polymerized, generating networks with branch and hexagon structures. e-3) Magnified images clearly demonstrate two types of molecular interconnection, highlighted by solid black and dashed blue circles and denoted by I1 and I2, respectively. e-4, e-5) High-resolution images (left) and molecular orbitals (right) of the two patterns. I1 and I2 correspond to symmetric 1,3,5- and asymmetric 1,2,4-trisubstitutions, respectively. Reproduced with permission.[255] Copyright 2014, American Chemical Society. f) Acetyl cyclotrimerization reaction. g) Representative STM image g-1) and magnified image g-2) after deposition with the substrate held at 590 K. Scanning parameters of c to e are V_b =1 V and It = 20 pA. Structural model h) and reaction product i) of the trifunctional acetyl compounds (newly formed phenyl ring highlighted in blue). Reproduced with permission.[256] Copyright 2015, American Chemical Society.

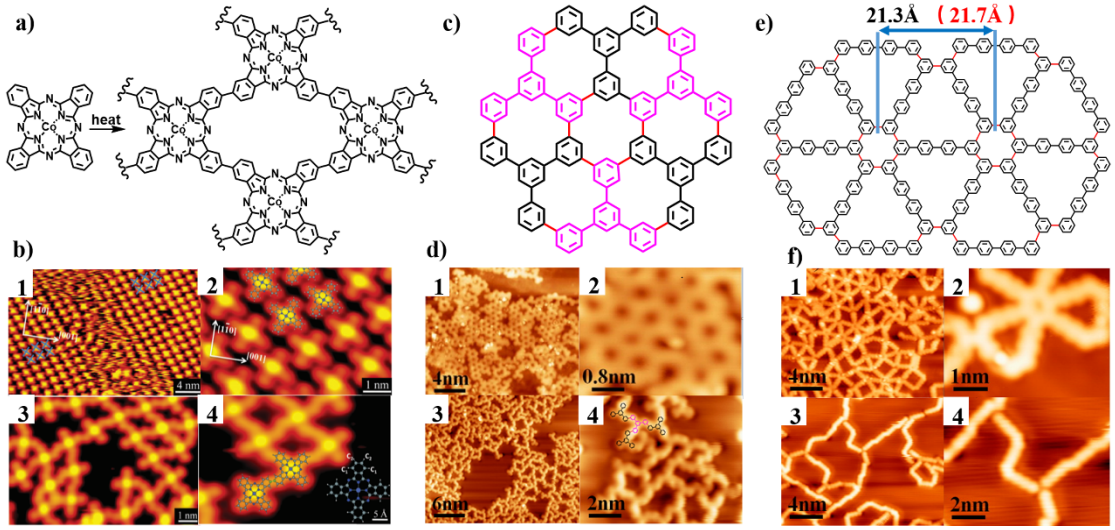

Figure 16. a) Chemical structure of the CoPc molecule and the formed 2D polymer structure. Large-scale b-1) and close-up STM images b-2) of the self-assembled CoPc structure on Ag (110). STM image b-3) and close-up STM image b-4) of the 2D polymer structure. Reproduced with permission.[259] Copyright 2015, Royal Society of Chemistry. c, d) Structural models c), STM images d-1, d-3), and close-up STM image d-2, d-4) of THPB on Au (111) and Ag (111) surfaces. e, f) Structural models e), STM images e-1, e-3), and close-up STM image e-2, e-4) of dihydroxy-*p*-quaterphenyl (DHQP) f) on Au (111) and Ag (111) surfaces. Reproduced with permission.[260] Copyright 2016, American Chemical Society.

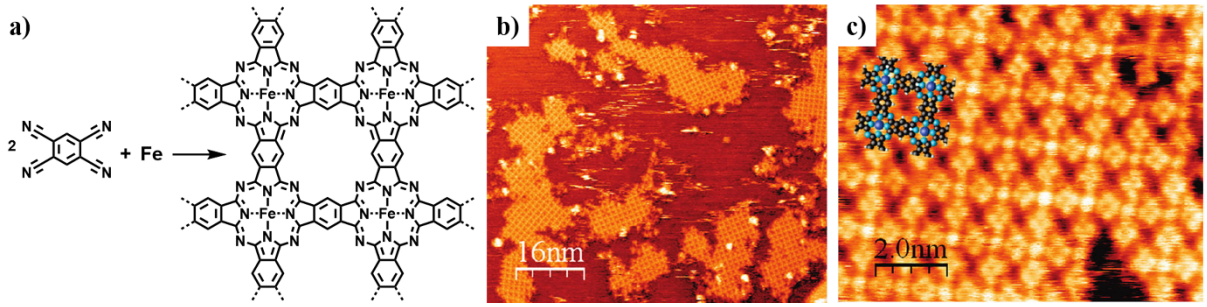

Figure 17. a) Synthesis reaction 2D iron phthalocyanine organometallic polymer (poly-FePc). b, c) STM images of poly-FePc formed on an Ag (111) surface (square unit cell, 1.15 nm large). Reproduced with permission.[261] Copyright 2011, American Chemical Society.

Jialing Kang received her bachelor degree in polymer materials and engineering from Hengyang Normal University in 2017. She is currently pursuing her master degree at the Shanghai Institute of Technology and working as an exchange student in Prof. Zhuang's group. Her topic is rational design and synthesis of 2D conjugated porous polymers and porous carbons with well-defined active sites for energy conversion.

Feng Qiu obtained his Ph.D. from Shanghai Jiao Tong University under the supervision of Prof. Xinyuan Zhu in 2013. He then did his postdoctoral research at Shanghai Jiao Tong University and University of Bristol. Now, he worked at Shanghai Institute of Technology as an associate professor from 2018. His current research interests focus on the controlled preparation of 2D nanostructures from functional polymers and their energy applications.

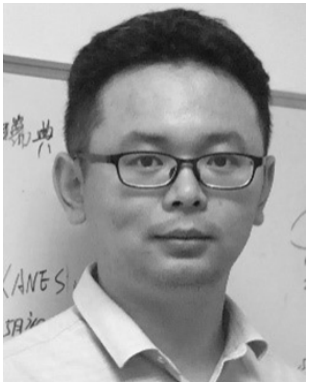

Xiaodong Zhuang, a synthetic material chemist, is presently a full professor of Shanghai Jiao Tong University and the head of The Meso-Entropy Matter Lab. He has been awarded NSFC Excellent Young Scientists, IAAM Medal Award, RSC Emerging Investigator, MoE Science Award II, CCS Chinese Young Chemists, etc. Zhuang's scientific interests include rational designed meso-entropy matter, including 2D soft materials and carbon-rich materials, for energy storage and conversion.